Physics and Chemistry of Minerals (2022) 49:32
https://doi.org/10.1007/s00269-022-01207-4

ORIGINAL PAPER

GeoSoilEnviroCARS (Sector 13) at the Advanced Photon Source: a comprehensive synchrotron radiation facility for Earth science research at ambient and extreme conditions

S. R. Sutton[1] · M. L. Rivers[1] · S. Chariton[1] · P. J. Eng[1] · A. Lanzirotti[1] · M. Newville[1] · T. Officer[1] · V. B. Prakapenka[1] · Y. J. Ryu[1] · J. E. Stubbs[1] · S. Tkachev[1] · Y. Wang[1] · A. Wanhala[1] · J. Xu[2] · M. Xu[1] · T. Yu[1] · D. Zhang[2]

Received: 21 March 2022 / Accepted: 21 June 2022
© The Author(s), under exclusive licence to Springer-Verlag GmbH Germany, part of Springer Nature 2022

Abstract

GeoSoilEnviroCARS (GSECARS) is a comprehensive analytical laboratory for Earth and environmental science research using X-ray beams from the Advanced Photon Source, Argonne National Laboratory. State-of-the-art instruments are available for (1) high-pressure/high- or low-temperature diffraction, total scattering, and spectroscopy (Brillouin, Raman, and VIS-IR) using the laser heated diamond anvil cell (DAC); (2) high-pressure/high-temperature diffraction, scattering, and imaging as well as acoustic emission (AE) and ultrasonics using the large-volume press (LVP); (3) powder, single crystal, and surface/interface diffraction; (4) X-ray absorption fine structure spectroscopy; (5) X-ray fluorescence microprobe analysis; and (6) microtomography. Experiments are facilitated by senior level staff who collaborate on all aspects of the analytical work including experiment design, sample preparation, data collection, data interpretation, and publication preparation. Both technical and scientific synergies occur as a result of the intimate association of the various techniques and scientists experienced in the applications of synchrotron radiation to Earth, environmental, and planetary science problems. The facility includes state-of-the-art instrumentation designed and built in-house, including custom X-ray optics, online and offline laser-based systems, specialized sample environments and positioning systems, as well as pixel-array and multi-crystal energy dispersive X-ray detectors, which are available to be shared among the experimental stations.

Keywords Synchrotron radiation · X-ray analytical methods · User facilities · Geochemistry · Geophysics

Introduction

GeoSoilEnviroCARS (GSECARS) is a national user facility at the Advanced Photon Source (APS, Argonne National Laboratory, USA) dedicated to frontier research in the Earth, environmental and planetary sciences. GSECARS was designed and constructed as a community facility, beginning in 1994. The design was a community effort supported by five design teams, consisting of leaders in the field of each technique: (1) Diamond anvil cell (DAC), (2) Large volume press (LVP), (3) X-ray diffraction and scattering, (4) X-ray absorption spectroscopy and anomalous scattering, and (5) X-ray fluorescence microprobe and microtomography. Most principal synchrotron-based analytical techniques in demand by scientists and students in these fields are available for use (Table 1).

High-pressure, high-temperature devices are available to study the properties of candidate core and mantle materials under relevant conditions. The diamond anvil cell, with both laser and external heating, can reach pressure and temperature conditions present in the interiors of the Earth and other planets with diffraction and spectroscopic methods applicable for determining equation of state, melting behavior, structure, phase relations, chemical reactions and kinetics, transport, elastic, electronic and optical properties of a wide range of minerals. Multi-anvil presses coupled

---

This article is part of a Topical Collection "Experimental & Analytical Techniques at Extreme & Ambient Conditions", guest edited by Stella Chariton,Vitali B. Prakapenka and Haozhe (Arthur) Liu".

S. R. Sutton
sutton@cars.uchicago.edu

[1] Center for Advanced Radiation Sources, The University of Chicago, Chicago, IL, USA

[2] Hawai‘i Institute of Geophysics and Planetology, University of Hawai‘i at Mānoa, Honolulu, HI, USA

Published online: 26 July 2022

Table 1 Summary of GSECARS experimental stations, their instruments, available techniques, and some specifications

Station	Instrument	Technique	Energy Range (keV)	Beam size (µm)	X-ray optics	Primary X-ray detectors
13-ID-E	X-ray Microprobe	Trace element microanalysis, fluorescence microtomography, microXAFS, microdiffraction, HERFD	2.4–28	1–2	Si(111), Si(311), KB mirrors	7-channel Si drift, HERFD analyzer, Eiger2 S 1 M
13-ID-C	General Purpose Diffractometer	Surface and interface scattering, grazing incidence XAFS, inelastic X-ray scattering	5–75	30×30	Si(111), Si(311), KB mirrors (1 m)	Pilatus 100 k, 1 M; Vortex ME4
		Paris-Edinburgh high pressure cell	5–75	30×30	Si(111), Si(311), KB mirrors (1 m)	Pilatus3 X CdTe 300 K-W
13-ID-D	Laser-heated Diamond Anvil Cell	Monochromatic diffraction, emission spectroscopy	5–75	3×3	Si(111), Si(311), KB mirrors	Pilatus3 X CdTe 1 M
	Multi-anvil Press (1000 T)	Monochromatic & energy dispersive diffraction, ultrasonics, acoustic emission	5–75 white	30×30	Si(111), KB mirrors (1 m)	Pilatus 100 k, Canberra 16-element Ge
		Radiography	white	3×1 mm	Si(111), KB mirrors (1 m)	Princeton Instruments visible light CCD
13-BM-D	Multi-anvil Press (250 T)	Monochromatic & energy dispersive diffraction, ultrasonics, acoustic emission	5–90	4×12	Horiz. mirror (200 mm), Vert. mirror (1 m), Si(111)	Pilatus 100 k, Canberra 16-element Ge
		Tomography & radiography	5–90 white	50×4 mm	Vert. mirror (1 m), Si(111)	Pilatus 100 k, Canberra 16-element Ge
	Diamond Anvil Cell	Brillouin spectroscopy, monochromatic diffraction	5–90	4×12	Horiz. mirror (200 mm), Vert. mirror (1 m), Si(111)	Pilatus3 S CdTe 1 M
	Tomography	Absorption & phase contrast tomography	5–90 pink white	50×4 mm	Vert. mirror (1 m), Si(111)	Point Grey GS3-U3-23S6M USB-3 CMOS camera
13-BM-C	General Purpose Diffractometer	Diamond anvil cell diffraction	15, 28.6	12×18	Si(111) or Si(311) mono, horiz. mirror (320 mm), vert. mirror (1 m)	Pilatus 100 k, 1 M
		Surface and interface diffraction, powder diffraction	15, 28.6	30×300	Horiz. focusing mono Si(111) or Si(311), Vert. focusing mirror (1 m)	Pilatus 100 k, 1 M

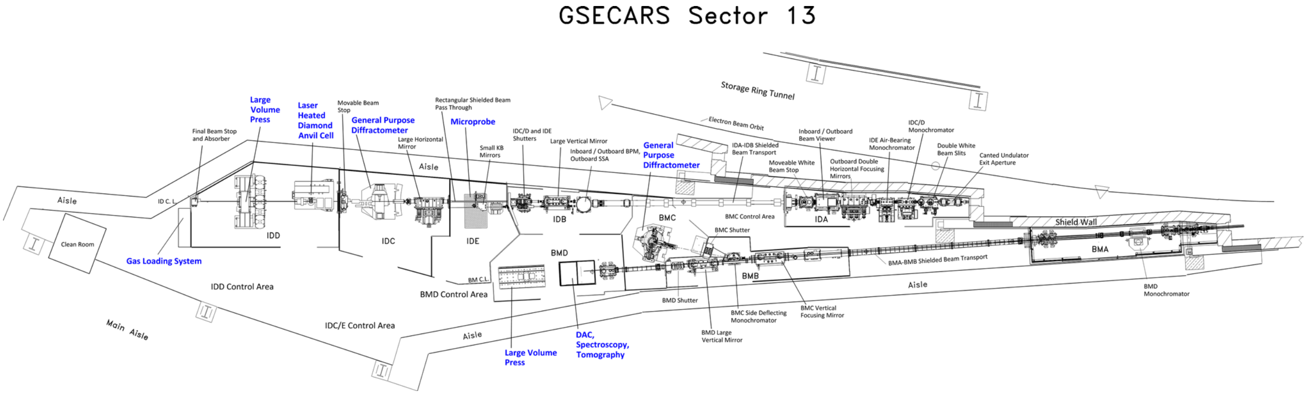

Fig. 1 Layout of the GSECARS sector (13) at the Advanced Photon Source, Argonne National Laboratory, USA

with differential rams, diffraction, tomographic imaging, ultrasonics, and acoustic emission (AE) methods provide a versatile approach to explore the structural and rheological properties of Earth materials that are the foundations for geodynamic modeling. Both types of high-pressure instruments are applicable to samples covering the entire range of crystallinity from single crystals to amorphous materials and melts. General purpose diffractometers are available for single crystal and powder diffraction, surface and interface scattering, and grazing-incidence spectroscopy. These complementary techniques allow studies of chemical interactions at interfaces between minerals and aqueous solutions, reactions that often dominate the fate and transport of trace elements and pollutants within the Earth's hydrosphere. X-ray microprobe techniques are used for fundamental geochemical studies of the complex heterogeneous systems applying X-ray fluorescence, X-ray absorption fine structure spectroscopy, diffraction, and tomography with micrometer spatial resolution. The absorption tomography system can be used for the non-destructive study of the internal structures of samples such as fossils, the distribution and location of inclusions in diamonds, the porosity and density of weathered rocks, studies of granular flow, and the transport of fluids such as water and oils in porous media. Raman and optical spectroscopy in combination with X-ray techniques provide a powerful approach for acquiring the multi-faceted data needed to develop realistic models of how the interior and surface of the Earth and other planets formed, evolved, and currently operate.

Because of the all-encompassing nature of the facility, GSECARS can be considered a comprehensive analytical laboratory consisting of four beamlines with a total of five experimental stations. Senior level staff with extensive experience in both Earth science and instrumentation development are available at each instrument to collaborate on all aspects of the analytical work including experiment design, sample preparation, data collection, data interpretation, and publication preparation. The science program is largely driven by the high-impact experiments defined by our users in collaboration with GSECARS staff that in turn are driven by funding agency priorities and support to these individual investigators. The intimate association of the various techniques leads to synergistic developments in instrumentation, analytical capabilities, and scientific projects. A suite of state-of-the-art X-ray detectors, including pixel-array and multi-crystal energy dispersive detectors, are available to be shared among the experimental stations.

Sector overview

GSECARS is a sector (a storage ring port with both insertion device and bending magnet sources) at the APS (Fig. 1). The sector consists of canted undulator (i.e., two insertion devices) beamlines (13-ID), a split bending magnet beamline (13-BM), and five support laboratories. Each beamline consists of a first optics enclosure (13-ID-A and 13-BM-A), second optics enclosure (13-ID-B and 13-BM-B), and experimental stations (13-ID-C, 13-ID-D, 13-ID-E, 13-BM-C, and 13-BM-D). Four of the five experimental stations operate simultaneously: 13-BM-C, 13-BM-D, 13-ID-E, and 13-ID-C or 13-ID-D. The bending magnet fan is divided into two parts. An outboard fan of 2.5 mrad feeds the 13-BM-D station, and an inboard fan of 1.5 mrad feeds the 13-BM-C station. These fans are separated by 1 mrad. The extreme inside and outside 0.5 mrad on each edge of the 6 mrad fan is not used. The primary techniques, instrumentation, and science areas available in each station are summarized in the following sections.

Diamond anvil cell high-pressure diffraction and spectroscopy

Stations: 13-ID-D, 13-BM-C, 13-BM-D and offline laser laboratory.

Techniques: Monochromatic non-crystalline, powder, and single-crystal diffraction, Emission spectroscopy, Brillouin and Raman spectroscopy.

Technical description: Diamond anvil cell (DAC) high-pressure experiments are conducted in three stations. The DAC instrument in the 13-ID-D end station (Fig. 2) uses a 3.0 cm period undulator as an X-ray source. The monochromator is a cryogenically cooled, Si (111) or Si (311), fixed offset, double-crystal instrument operating between 5 and 75 keV. Dynamically bent, Kirkpatrick-Baez (KB) mirrors (200 mm Si, Pt coated) are used to focus the beam to ~3 µm diameter and a pinhole is used to block the wings of this microfocused beam. The 13-ID-D standard setup allows collecting diffraction data in situ at extreme pressure and temperature in static and time-domain modes including with the DAC in a cryostat coupled with compression membrane. The ~1 µm wavelength fiber lasers for double-sided laser heating are equipped with flat-top shaping optics ensuring a uniform heating spot of 10–30 µm on both sides (Prakapenka et al. 2008). These lasers can be operated in continuous or pulsed mode with repetition rates up to 50 kHz. A CO_2 laser (~10 µm wavelength) provides efficient heating of substances transparent to the near IR light (~1 µm wavelength) without the need for a light absorber. Temperature is estimated by fitting the thermal radiation spectrum to the Planck radiation function. Most experiments utilize a Dectris Pilatus3 X CdTe 1 M pixel array detector (shared with ChemMatCARS Sector 15). An alternative setup allows X-ray emission spectroscopy (XES) measurements at high temperature and high pressure in the laser heated DAC to probe the spin-state of iron in mineral-forming iron-bearing phases. X-ray emission of the iron $K_{\beta 1,3}$ line is probed using a Si 440 analyzer coupled with the Pilatus 100 K Si detector held in a fixed position allowing energy scanning between 7018 and 7078 eV.

The 13-BM-D bending magnet station has a non-focusing, water-cooled, Si (111) double-crystal monochromator that covers the energy range from ~5 to 90 keV. A 1-m long mirror in the 13-BM-B optics station is used for vertical focusing. A 200 mm KB mirror is placed on the experimental table for horizontal focusing to a spot ~4×12 µm ($H \times V$). XRD measurements use a Pilatus3 S 1 M CdTe pixel array

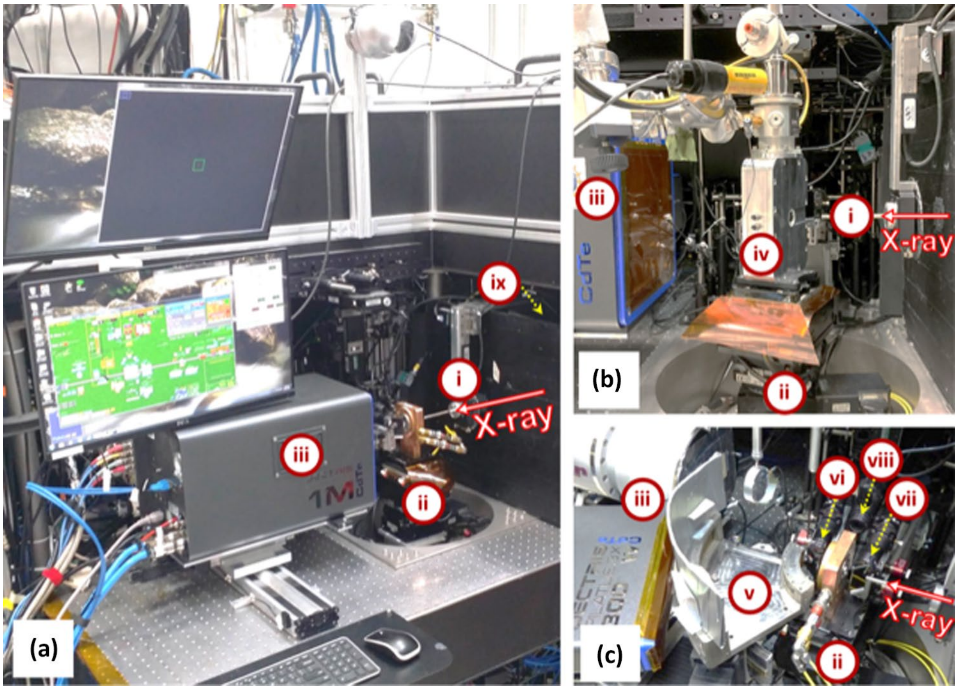

Fig. 2 **a** The laser-heated diamond anvil cell apparatus in station 13-ID-D. The station hosts **b** low-temperature experiments in a customized cryogenic enclosure, as well as, **c** total X-ray scattering experiments using the multichannel collimator setup (i = pinhole; ii = X–Y–Z–ω stack of sample stages; iii = X-ray detector (in **a** and **b**, Pilatus3 X 1 M CdTe and in **c**, Pilatus3 X 300 K CdTe or MAR165 CCD); iv = Cryostat enclosure for laser-heated DACs with compression membrane controller; v = multichannel collimator; vi and vii = downstream and upstream objectives for laser heating, respectively; viii = optical microscope; ix = enclosure for horizontal and vertical focusing KB mirrors). The system includes online Raman and VIS-IR spectroscopy

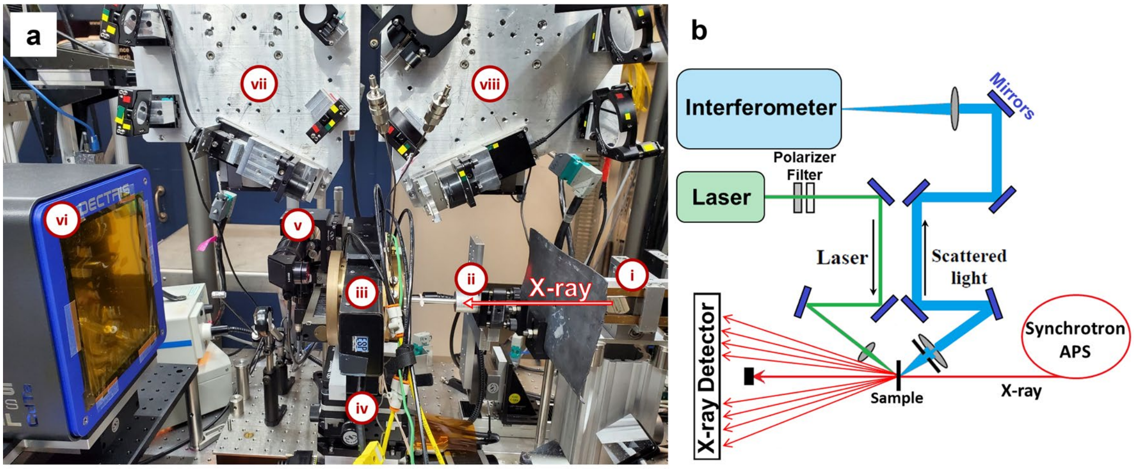

Fig. 3 **a** Diamond anvil cell apparatus with Brillouin spectroscopy system in station 13-BM-D (i = horizontal focusing KB mirror; ii = pinhole; iii = a vacuum enclosure with double-stage membrane pressure controller and resistive-heating setup is shown mounted on a chi-rotational stage; iv = X–Y–Z–ω stack of sample stages; v = optical microscope; vi = Pilatus 3 S 1 M CdTe X-ray detector; vii = optical path for Brillouin system's laser to the sample; viii = optical path of the samples' scattered light to the interferometer). **b** Schematic of Brillouin spectroscopy optical paths. The system includes online Raman and VIS-IR spectroscopy

detector. The XRD DAC setup includes Brillouin and Raman spectroscopy systems for measurement of elastic and optical properties at high pressure and high temperature in the externally heated DAC (Sinogeikin et al. 2006a) (Fig. 3).

The 13-BM-C beamline (Fig. 4), shared with the PX^2 partnership managed by the University of Hawaii, has a focusing Si (111) and Si (311) single-crystal, side-bounce monochromator operating at two fixed energies, Si (111) is used at 15 keV whereas the Si (311) is used at 28.6 keV. There is a 1-m long vertical focusing mirror in the 13-BM-B optics station which is used for vertical focusing, and a 320-mm long KB mirror that is placed on the entrance bench in 13-BM-C for horizontal focusing in DAC experiments, with a final focal size of ~12 × 18 m ($H \times V$). A Pilatus3 S 1 M pixel array detector with 1-mm thick Si sensor is used for high-pressure XRD measurements, and a miniature optical platform is installed for sample observation, ruby fluorescence, and laser heating (https://link.springer.com/article/10.1007/s00269-022-01197-3).

A GSECARS laser laboratory is adjacent to the experimental stations and is equipped with laser ultrasonic and high-resolution integrated optical systems. Optical

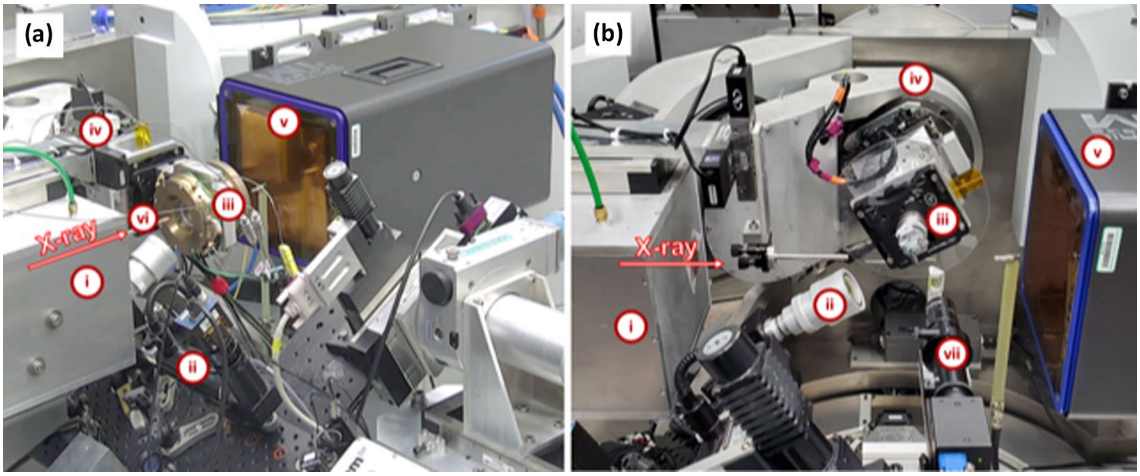

Fig. 4 The 6-circle diffractometer in station 13-BM-C used for **a** diamond anvil cell experiments, and **b** free-standing samples such as diamond inclusions (i = horizontal KB focusing mirror enclosure; ii = miniature optical platform for sample observation, ruby fluorescence and laser heating; iii = sample stage, for DAC experiments a vacuum enclosure with double-stage membrane pressure controller and resistive-heating setup is shown; iv = 6-circle goniometer; v = Pilatus3 S 1 M Si X-ray detector; vi = X-ray clean-up slit; vii = portable X-ray radiography setup)

spectroscopy performed on the same sample as studied by X-ray diffraction and at the same P–T conditions greatly enhances the quality of this research and, moreover, provides unique new information on the chemical state of matter. We have built an integrated optical system with five excitation wavelengths (266, 473, 532, 660, and 946 nm) for Raman spectroscopy, confocal imaging, double-sided IR laser heating combined with high temperature Raman (including coherent anti-Stokes Raman scattering) and transient (based on a bright supercontinuum light source) spectroscopies in a wide spectral range (200–1600 nm) (Holtgrewe et al. 2019a).

To study elastic properties of opaque minerals in situ at high pressure and temperature, we have combined laser ultrasonic and laser heating techniques allowing shear and longitudinal wave velocities to be measured under extreme conditions. A 532-nm, 150 mW continuous laser is used as the probe in combination with the Nd:YAG (1064 nm) pulsed laser (pulse width of 0.5 ns at frequency of 1 kHz). A photodetector with a bandwidth of 1 GHz and a LeCroy WavePro 725Zi oscilloscope are used to record photoacoustic signals in time domain mode (Zinin et al. 2016).

Science areas: The GSECARS DAC instrumentation is utilized for a wide range of experiments related to the composition of the Earth's mantle and core and the processes at work in the deep Earth and other planets including equations of state and phase stability, element partitioning, accurate structural determinations, elasticity, rheology, kinetics of phase transformations, and chemical reactions at extreme conditions. Measuring the phase equilibria, transport, and elastic properties of minerals in situ at high pressure using a combination of X-ray, electrical conductivity, and optical probes combined with ex-situ characterization of sample texture (e.g., microtomography) and composition provides a powerful approach for acquiring the multi-faceted data needed to develop realistic models of how the interiors of the Earth and other planets formed, evolved, and currently operate. The GSECARS DAC program allows the study of materials with cutting-edge tools under in-situ high-pressure and high/low-temperature conditions in the static or time domain modes to address the fundamental questions of evolution and structure of the Earth and other planetary bodies' interiors (Prakapenka et al. 2005, 2008; Sinogeikin et al. 2006b; Goncharov et al. 2010; Kantor et al. 2012; Dera et al. 2013; Prescher and Prakapenka 2015; Zinin et al. 2016; Holtgrewe et al. 2019b; Lai et al. 2020; Hong and Newville 2020). Selected science areas with examples of the most recent publications include the following:

Hydrous systems in the deep planetary interiors. The amount of hydrogen stored in the deep Earth and planetary interiors is important for a range of questions, including the chemical stability of minerals, phase relations, and volatile incorporation during planetary formation. Combined synchrotron X-ray diffraction and optical spectroscopy measurements of H_2O in the laser-heated DAC up to 150 GPa and 6500 K reveal first-order transitions to ices with body-centered cubic and face-centered cubic oxygen lattices assigned to superionic phases based on the abrupt changes in density and optical conductivity at phase transitions (Prakapenka et al. 2021). P–T stability fields of superionic phases and the melting line suggest that these types of ice-forms exist at conditions deep inside water-reach planets like Neptune and Uranus and may play important roles in a planet's magnetic fields formation (Fig. 5). A new hydrous iron oxide (η-$Fe_{12}O_{18+x/2}H_x$; $x \sim 2$) was shown to exist together with the major lower mantle minerals including bridgmanite (Brd) and periclase (Fp), making it an important hydrogen-bearing phase in the Earth's deep interior (Chen et al. 2020c). Hydrous ringwoodite converts to crystalline dense hydrous silica, stishovite (Stv) or $CaCl_2$-type SiO_2, containing 1 wt. % H_2O together with Brd and MgO at the pressure–temperature conditions expected for shallow lower mantle depths between approximately 660 and 1600 km. The results may provide an explanation for the enigmatic coexistence of Stv and Fp inclusions in lower mantle diamonds (Chen et al. 2020b). Formation of separate delta-AlOOH and hydrous

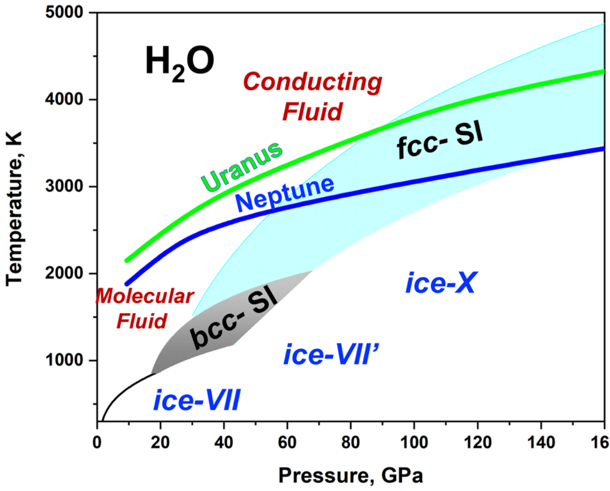

Fig. 5 Phase diagram of water derived from XRD experiments at high temperature and pressure in the diamond anvil cell (Prakapenka et al. 2021) compared to calculated isentropes of Neptune (blue line) and Uranus (green line; Redmer et al. 2011). The gray field labeled "bcc-SI" corresponds to the stability field of the body-centered-cubic superionic phase. The teal field labeled "fcc-SI" corresponds to the stability field of the face-centered-cubic superionic phase. Note the abrupt change in the slope of the melting line in the pressure stability range of both superionic phases. At low temperature, the solid phase is either ice-VII, ice-VII', or ice-X, depending on pressure. The fluid is either molecular ionic or conducting, depending on pressure. These results suggest the presence of face-centered cubic superionic ice in water-rich giant planets, such as Neptune and Uranus. Adapted from Prakapenka et al. (2021)

$CaSiO_3$ perovskite (Ca-Pv) phases from Al-bearing $CaSiO_3$ glass starting materials in an H_2O medium at 60 GPa and 1400 K, indicates that hydrous phases may coexist with hydrous Ca-Pv in the lower mantle (Chen et al. 2020a). Partial melting could be triggered by dehydration of the Fe-bearing hydrous phases due to a steep temperature gradient at the core-mantle boundary (CMB), and therefore the ultralow-velocity zones (ULVZs) might be the regions where partial melting occurs in the lowermost mantle (Yuan et al. 2019).

Carbon bearing minerals. The ability of carbon to form sp^2 and sp^3 bonds leads to structural and chemical diversity of carbon-bearing phases at extreme conditions. The single-crystal X-ray diffraction measurements using synchrotron radiation allowed the structure of carbonates to be determined with high precision on atomic positions, bond lengths, and bond angles. The laser-heated synthetic $(Mg_{0.85}Fe_{0.15})CO_3$ single crystal at 2500 K and 98 GPa transforms to a monoclinic phase with composition $(Mg_{2.53}Fe_{0.47})C_3O_9$, indexed in the C2/m space group that contains tetrahedrally coordinated carbon (Chariton et al. 2020). Dolomite $(Mg, Ca)CO_3$ and iron at pressure and temperature conditions of the deep lower mantle show that carbon-iron redox interactions destabilize the $MgCO_3$ component, producing a mixture of diamond, Fe_7C_3, and (Mg, Fe)O. This transformation constrains the thermodynamic stability of redox-driven breakdown of carbonates and demonstrates progress toward multi-phase mantle petrology at the lowermost mantle (Dorfman et al. 2018). Other experiments (Lv et al. 2021) demonstrate that, at deep mantle conditions, $MgCO_3$ reacts with silicates to form $CaCO_3$, which allows us to predict that the signature of surface carbon reaching Earth's lowermost mantle may include $CaCO_3$ with implications for deep mantle chemistry.

Elastic properties. The knowledge of elasticity of minerals measured in situ at high P–T conditions help to address important key questions in geoscience: composition of Earth's mantle/core, plate subductions, origin of seismic heterogeneities. Combining Brillouin spectroscopy with high resolution synchrotron X-ray diffraction techniques allows simultaneous measurements of sound velocities, elastic moduli, and the volume/density, independent of any pressure standard. Direct experimental measurements with Brillouin spectroscopy provide constraints on the single-crystal elasticity of salty ice up to 98 GPa at 300 K (Shi et al. 2021). The transition from ice-VII to the dynamically disordered phase and then to ice X is characterized by the anomalous variation in all the elastic constants followed by a change in the pressure gradient of the elasticity. These results provide important information for the internal structure of icy planetary bodies. The combined effects of pressure and temperature on the elastic moduli of single-crystal periclase using third-order Eulerian finite-strain equations showed that elastic moduli increased with increasing pressure but decreased with increasing temperature, except the off-diagonal modulus C-12, which remained almost constant up to 30 GPa and 900 K (Fan et al. 2019). The modeling results showed that both the increase in the Fe content in Fp and the increasing depth could change the compressional wave anisotropy and shear wave splitting anisotropy of Fp in the upper parts of the lower mantle suggesting that Fe-induced lateral heterogeneities can significantly contribute to the observed seismic lateral heterogeneities in the Earth's lower mantle (670–1250 km).

Melting. One of the most challenging experiments in the DAC is the precise determination of the melting temperatures (Shen et al. 2004; Prakapenka et al. 2008). The instrumental sensitivity for probing a small amount of melt at the solidus was improved using the multichannel collimator thus allowing the detection of diffuse X-ray scattering. Diffuse scattering from a pyrolitic melt determined an anhydrous melting temperature of 3302 ± 100 K at 119 ± 6 GPa and 3430 ± 130 K at the CMB conditions, as the upper bound temperatures, suggesting that the CMB temperature is approximately 700 K lower than previous estimates (Kim et al. 2020). The high P–T melting experiments on $(Mg_{0.86}Fe_{0.14})O$ up to 120 GPa and 5400 K in the laser-heated DAC showed that low-spin (Mg, Fe)O exhibits 6–8% lower solidus and liquidus temperature than its high-spin counterpart and iron preferentially partitions into melt within the spin crossover to generate iron-rich low-spin melt (Fu et al. 2018), which could provide plausible explanations for the characteristic seismological signatures.

Multi-anvil press high-pressure diffraction and imaging

Stations: 13-ID-D, 13-BM-D, 13-ID-C.

Techniques: Energy dispersive diffraction, Monochromatic diffraction, Radiography, Tomography, Acoustic emission, Ultrasonics.

Technical description: The 1000 T large volume press (LVP) in the 13-ID-D end station uses a 3.0 cm period undulator as an X-ray source. The monochromator is a cryogenically cooled, Si (111), fixed offset, double-crystal instrument operating between 5 and 75 keV (Fig. 6). White beam energy dispersive measurements and imaging are also available**.** Two high-pressure modules are used in this LVP interchangeably: (1) T-25, a split-cylinder type Kawai apparatus that uses 25.4 mm second-stage WC anvils, with

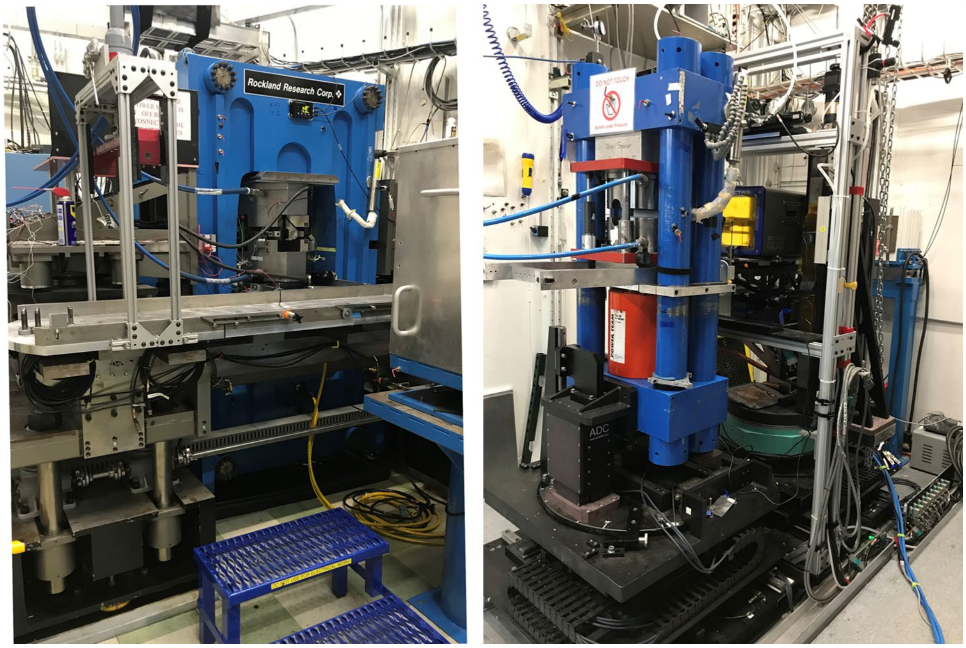

Fig. 6 Left: 1000 T LVP in station 13-ID-D. Includes T-25 module, DDIA-30, ultrasonics, acoustic emission, and electrical conductivity. Right: 250 T LVP in 13-BM-D. Multiple techniques are available, including D-DIA controlled deformation, high pressure tomography, ultrasonics, and acoustic emission

compression along the [111] axis of the Kawai cell. Maximum attainable pressure and temperature are 28 GPa and 3000 K, respectively. Standard cell assemblies: 8/3, 10/5, 14/8. (2) DDIA-30, a large deformation DIA which can be operated in two modes. In deformation mode, one may use 6-6MA cells (Nishiyama and Wang 2009) with desired anvil truncation to conduct deformation experiments, with strain and stresses controlled by the differential rams. In double-stage hydrostatic mode, one can use second-stage anvils made of sintered diamond anvils (14 mm cubes) for ultra-high-pressure experiments. Maximum pressure and temperature are currently 40 GPa and 2500 K, respectively. Acoustic interferometry is available for both modes. AE experiments are possible with the 6-6MA cell(s). More information can be found in Wang et al. (2009).

Multi-anvil experiments can be performed with a 250 T LVP in station 13-BM-D (Yu et al. 2019b) using the same beamline components as the DAC. Several configurations of the press are available based on the “Swiss-Army Knife” approach. (1) DIA apparatus, ideal for viscosity and density measurements based on X-ray absorption. (2) D-DIA for controlled deformation experiments. (3) high-pressure tomography apparatus for 3D sample microstructural imaging. (4) T-10, a smaller version of T-25. Both white and monochromatic radiation can be used. Acoustic interferometry is available for most of the devices. AE experiments are possible with the D-DIA and the high-pressure tomography cell(s).

The 230 T Paris-Edinburgh apparatus is utilized in 13-ID-C (collaboration with HPCAT Sector 16) for structural studies on amorphous materials using multi-angle

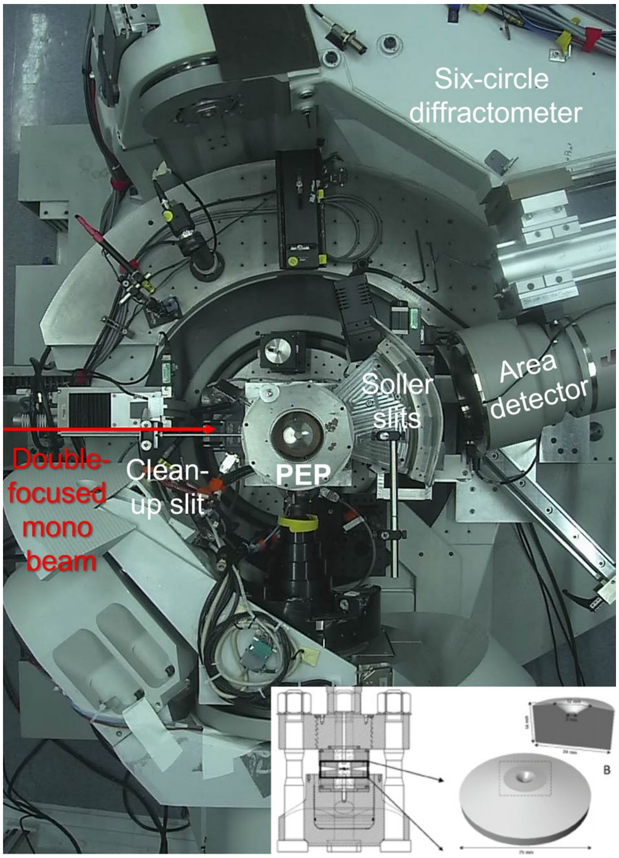

Fig. 7 Paris-Edinburgh cell on the diffractometer in station 13-ID-C (top view). Includes Soller slits for beam collimation. Inset (bottom right): Diagram of PE assembly

energy-dispersive diffraction (Fig. 7). Acoustic interferometry can be combined with diffraction.

Science areas: Advantages of LVPs in high-pressure studies include (1) large sample size, (2) minor and well-characterized pressure and temperature gradients, and (3) P–T paths that are well-controlled. Science areas include phase relations, combined P–V–T and acoustic velocity measurements for redundant equation of state determination, viscosity of melts, deformation studies with quantitative stress, strain, and strain rate information, melt curve definition, density and equation of state of non-crystalline materials, and high P–T crystallography.

Rheology of Earth materials at mantle P and T conditions. Deformation-DIA devices are used to explore the rheological properties of Earth materials, properties that are the foundations for geodynamic modeling. These capabilities are utilized to study the rheology of a wide range of minerals that are relevant to the mantle transition zone (MTZ) and lower mantle (Xu et al. 2020b). The GSECARS LVPs allow direct measurement of melt viscosities at high pressures using real-time X-ray radiography to monitor the fall of dense marker spheres through molten silicate melt (Tinker et al. 2004).

Mechanisms of deep focus earthquakes. The unique combination of D-DIA/DDIA-30 with AE allows systematic studies of phase transition triggered/induced failure mechanisms relevant to intermediate-depth and deep-focus earthquakes (Schubnel et al. 2013; Wang et al. 2017; Shi et al. 2018, 2022; Incel et al. 2019). Recent developments include modified anvils in DDIA-30 to reach 10+ GPa on large samples suitable for AE detection. This is critical for studying transformational faulting in silicate olivine, the “Holy Grail” of experimental investigation for deep focus earthquakes. Seismological methodology is applied for AE event location and waveform analyses, improving location resolution by a factor of > 10. Combined with X-ray microtomography imaging on recovered samples, AE distributions can be correlated with observed faulting in space and time.

Acoustic velocities and attenuation of transition zone, lower mantle, and core materials, as well as complex rock systems in the upper mantle (including partial melt systems). Four areas in this field are scientific foci (Jing et al. 2020). (i) Elasticity measurements of bridgmanite with various Al and Fe contents can help place tighter constraints on the lower mantle mineralogy (Chantel et al. 2012). (ii) Velocities of Fe–X (X = S, C, and O) liquids allow measurement of acoustic velocities of Fe-rich alloys in liquid state up to 10 GPa and beyond (Jing et al. 2014). Silicate and carbonate melts with sufficiently low viscosities have also been studied using this technique to determine relaxed elastic properties (Xu et al. 2020a, 2022) (iii) Measurement of both P and S waves allows determination of acoustic wave quality factor (Q) at the frequency range of our instruments (20–80 MHz) providing constraints on Q of minerals at seismic frequencies under realistic mantle P–T conditions (Chantel et al. 2016). (iv) Origin of the low-velocity zone (LVZ) can be studied via measurements on olivine + mid-ocean ridge basalt (MORB) assemblies at P–T conditions where MORB is molten (Chantel et al. 2016). Chemical interactions among all the components can be analyzed to correlate with velocity and Q measurements. Acoustic velocity, density, and viscosity measurements can be conducted on liquids in the LVP with ultrasonic interferometry, X-ray absorption, and falling-sphere techniques, respectively (Wang et al. 2009).

Properties of amorphous materials. Atomic-scale structures of silicate liquids control density and transport properties of magmas under pressure. Figure 8 shows a subset of techniques offered by the GSECARS LVP program for studying liquid properties. Liquid and amorphous structure measurements are also obtained using the total scattering technique in the Paris-Edinburgh press (Yu et al. 2019a).

Interface, single crystal, and powder diffraction

Stations: 13-ID-C, 13-BM-C.

Techniques: Crystal truncation rod (CTR), X-ray standing waves (XSW), reflectivity, grazing incidence X-ray fluorescence (GI-XRF), Grazing incidence X-ray absorption fine structure (GI-XAFS), Microcrystallography.

Technical description: The 13-ID-C beamline is equipped with a cryo-cooled double-crystal monochromator with either Si (111) or Si (311) crystal pairs; a pair of 1-m long Si mirrors in KB geometry for X-ray beam focusing (~30 × 30 μm), collimation, and harmonic rejection using Si, Rh, and Pt stripes; and a heavy-duty Newport 6-circle kappa diffractometer (Fig. 9). Scattered X-rays are detected using Dectris Pilatus 100 k or 1 M pixel array detectors with Si sensors. X-ray fluorescence spectra are collected using Vortex ME4 or single element, silicon drift diode detectors. The 13-ID-C monochromator can provide X-rays with energies between 5 and 75 keV, meaning elements heavier than vanadium should be accessible, although there are challenges associated with X-ray absorption by air, sample environments, beamline windows, etc. at the lower end of this energy range. The 13-BM-C beamline has a water-cooled Rowland circle monochromator that provides X-rays with either 15 or 28.6 keV energy and focuses the beam to 300 μm horizontally; a 1-m long Rh-coated Si mirror that

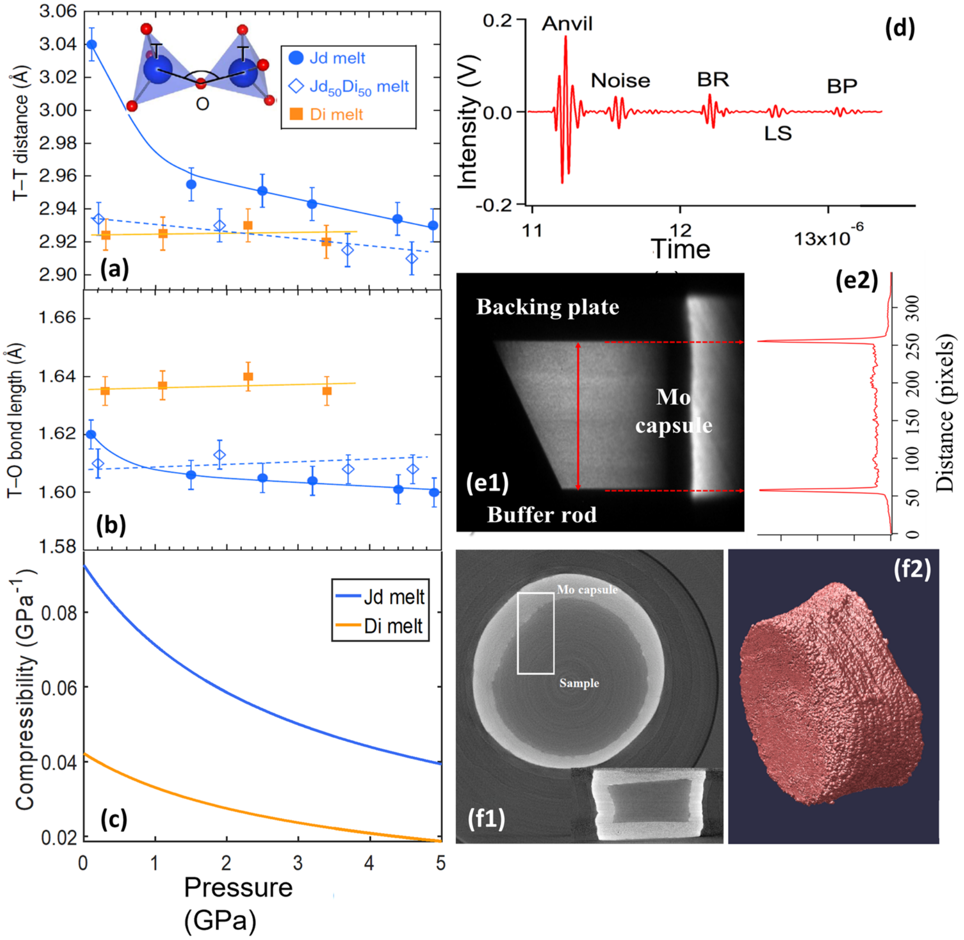

Fig. 8 Structure–property correlations in tetrahedrally coordinated silicate melts at high pressure. Two compositions are examined in detail: diopside (Di; $CaMgSi_2O_6$) and jadeite (Jd; $NaAlSi_2O_6$). While the former is a depolymerized liquid, with ~2 non-bridging oxygen (NBO) per tetrahedral unit (NBO/T = 2), the latter is a fully polymerized liquid with NBO/T = 0. The different connectivity of tetrahedra results in different response when the two liquids are compressed. **a** Si–Si (T-T) distance, determined by synchrotron X-ray scattering, as a function of pressure. For Di liquid, T-T distance is essentially independent of pressure. For Jd liquid, T-T decreases rapidly in a highly non-linear fashion. **b** Si–O (T-O) bond distance in Di and Jd liquids show similar contrast in pressure dependence. Both **a** and **b** are modified from Wang et al. (2014). **c** Compressibility of the two liquids as a function of pressure. Compressibility of Jd liquid is more than that of Di liquid and decreases more rapidly than that of Di. Data are from Xu et al. (2018, 2020b). The contrasting behavior is attributed to the degree of polymerization and voids in the two liquids (Wang et al. 2014). The two liquids also have very different viscosities, with contrasting pressure dependence. Viscosity of Jd is high (~10 Pa s at 1 bar) due to polymerization and decreases with pressure, reaching a minimum near 4 GPa before turning over at higher pressures. Viscosity of Di is much lower (~0.01 Pa s at 1 bar) and increases monotonically with pressure. The low viscosity of Di allows its relaxed elastic properties to be measured using ultrasonic techniques (Xu et al. 2018). **d** An example of liquid acoustic signal (LS) observed in Di liquid at 5 GPa and 2284 K. Round trip acoustic travel time is between LS and the buffer rod (BF) pulses. (e1) Radiographic image of the sample between the dark buffer rod and backing plate. (e2) Sample length is determined using intensity derivative of digitized image of (e1). Velocity is then determined based on travel time and sample length (Xu et al. 2018). For the viscous Jd liquid, ultrasonic technique cannot provide relaxed elastic information. Relaxed compressibility is determined using high-pressure microtomography (Xu et al. 2020b). (f1) Two cross sections of a reconstructed image of Jd liquid ("sample") in a Mo capsule at 3.7 GPa and 1934 K. (f2) Digitally extracted sample volume (Xu et al. 2020b). These results provide direct information on how pressure modifies liquid structure, resulting changes in physical properties

focuses the X-ray beam to 30 μm vertically; a diffractometer and detectors similar to those in the 13-ID-C instrument are utilized. The 13-BM-C instrument provides larger blocks of beamtime than at 13-ID-C, thus making it an excellent place to train new personnel and students, screen samples, prototype new sample environments, and test new preparation methods.

Science Areas: These experiments focus on chemical interactions at interfaces between solids and aqueous solutions, reactions that often dominate the fate and transport of trace elements and pollutants within the Earth's hydrosphere and are largely responsible for the trace element composition of the oceans, for example. A number of complementary surface-sensitive techniques are currently in place at GSECARS

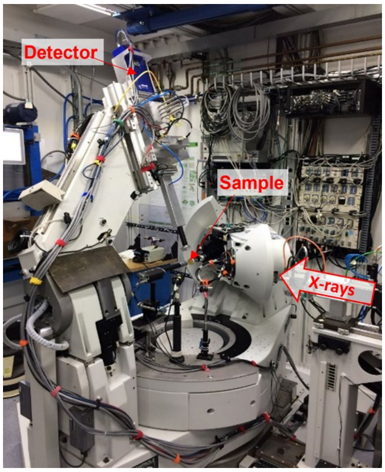

Fig. 9 General purpose 6-circle diffractometer in station 13-ID-C used for surface and interface scattering experiments

including; (1) crystal truncation rod (CTR) diffraction and grazing-angle reflectivity for the analysis of surface and interface structure; (2) resonant anomalous X-ray reflectivity (RAXR)—an element-specific form of CTR; (3) X-ray absorption fine structure and grazing-incidence absorption spectroscopy to probe the local structure and oxidation state of surface-bound species; (4) X-ray standing wave fluorescence-yield measurements for the determination of the position and distribution of surface and interfacial species; and (5) powder diffraction in complex sample environments, enabling time-resolved in-situ measurements with aqueous solution flow, heating, and electrochemical control of redox states. The GSECARS General Purpose Diffractometers allow a combination of these techniques to be applied on samples under in-situ conditions (i.e., in the presence of bulk solution or controlled atmosphere).

Mineral–water interfacial structures. Mineral–water interfacial structures have been determined for a variety of environmentally and economically important minerals, often coupling CTR measurements with computational methods (Bracco et al. 2017; McBriarty et al. 2017; Stack et al. 2018). Figure 10 shows an example where epitaxial growth of gibbsite-like sheets on muscovite is revealed via CTR (Stubbs et al. 2019). Adsorbate binding mechanisms and geometries have been revealed using CTR and RAXR for trace elements and potential contaminants including Pb, As, Sr, and Sb (Bracco et al. 2018; Qiu et al. 2018b, a; Xu et al. 2019). Custom electrochemical cells have enabled in-situ

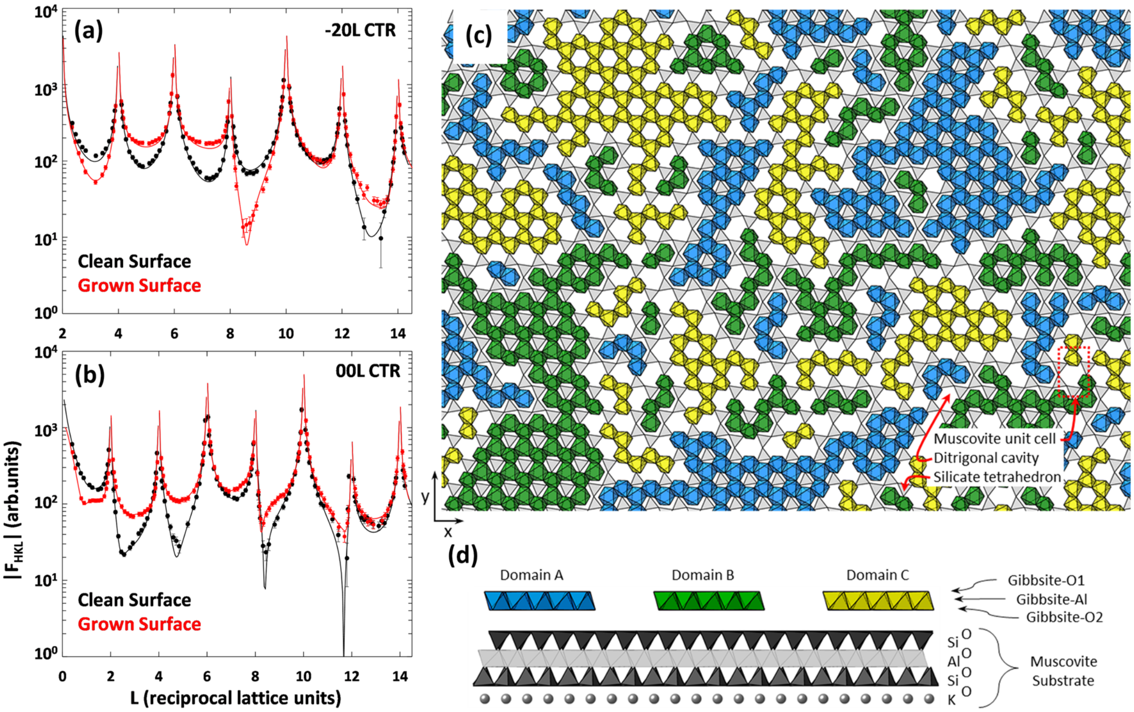

Fig. 10 Off-specular **a** and specular **b** CTR data collected from a muscovite mica surface after rinsing with DI water (black) and after reaction with 1 mM $AlCl_3$ solution at pH 4 (red). Symbols represent data and lines show best fits. Structural model fitting reveals that epitaxial gibbsite-like dioctahedral sheets grow in three structurally related domains that are one layer thick. In domains A, B gibbsite vacancies overlie muscovite silicate tetrahedra. In domain C they overlie ditrigonal cavities. Schematic representation of model with three gibbsite domains is shown perpendicular to the (001) surface **c** and along (010) **d**. Gibbsite octahedral occupancies in part c generated by Monte Carlo simulation (Figure adapted from Stubbs et al. 2019)

manipulation of interfacial redox reactions, including the flipping of water molecules (McBriarty et al. 2018a) and reductive dissolution of iron at hematite surfaces (McBriarty et al. 2018b). Surface and interface measurements involving radioactive materials have been enabled by the development of sample cells that meet the requirements of both surface scattering and radioactive containment (Schmidt et al. 2011; Stubbs et al. 2015; Neumann et al. 2021). New developments have extended structural analysis techniques to crystals < 300 µm in size, thereby expanding the suite of minerals to which CTR can be applied (Stubbs et al. 2021).

Non-single-crystal materials. Long period standing wave—fluorescence yield (LPSW-FY) measurements and grazing-XAFS enable investigation of biofilms, nanoparticles, and non-single-crystal materials at environmentally relevant interfaces. For example, Wang et al. (2016c, a, b) used these methods to explore the distribution of Pb, Cu, and Zn in biofilms and organic matter coatings and Desmau et al. (2018, 2020) investigated the interaction of silver nanoparticles and quantum dots with biofilm-coated minerals.

Reactions and transformations. In-situ powder diffraction capabilities enable the study of mineral-solution reactions and phase transformations in real time, including cation exchange in manganese oxides, growth conditions for iron oxides, and mineral dehydration reactions (Kong et al. 2019; Heaney et al. 2020; Chen et al. 2021). Kong et al. (2019) explored Cr oxidation with time-resolved XRD and Cr K-edge X-ray absorption near edge structure (XANES) while flowing Cr(III)-bearing solutions through capillaries packed with the triclinic form of the manganese oxide birnessite, and using visible-light spectrophotometry on effluent solutions to quantify Cr(VI) concentrations. These multi-modal measurements revealed extensive oxidation of dissolved Cr concomitant with transformation of triclinic to hexagonal birnessite, yielding critical insights into an important class of environmental reactions. New developments are underway to enable in-situ electrochemistry inside capillaries during time-resolved powder diffraction experiments, enabling the measurement of precisely controlled redox-driven structural transformations.

X-ray microprobe fluorescence, spectroscopy, and diffraction

Station: 13-ID-E.

Techniques: Micro-X-ray fluorescence (microXRF), Micro-X-ray absorption fine structure (microXAFS), Micro-X-ray diffraction (microXRD), fluorescence computed microtomography (FCMT), High energy-resolution fluorescence detection (HERFD).

Technical description: The X-ray microprobe (Fig. 11) uses a 3.6-cm period undulator and cryogenic, double-crystal monochromator using either Si(111) or Si(311) crystal pairs (greater energy resolution with the latter) as the X-ray source in the 2.4–28 keV range. Dual, horizontally deflecting, focusing mirrors increase the separation between the beam and the 13-ID-C/D beam in a canted insertion device geometry. These mirrors also create a secondary source image at the location of a secondary source aperture (SSA),

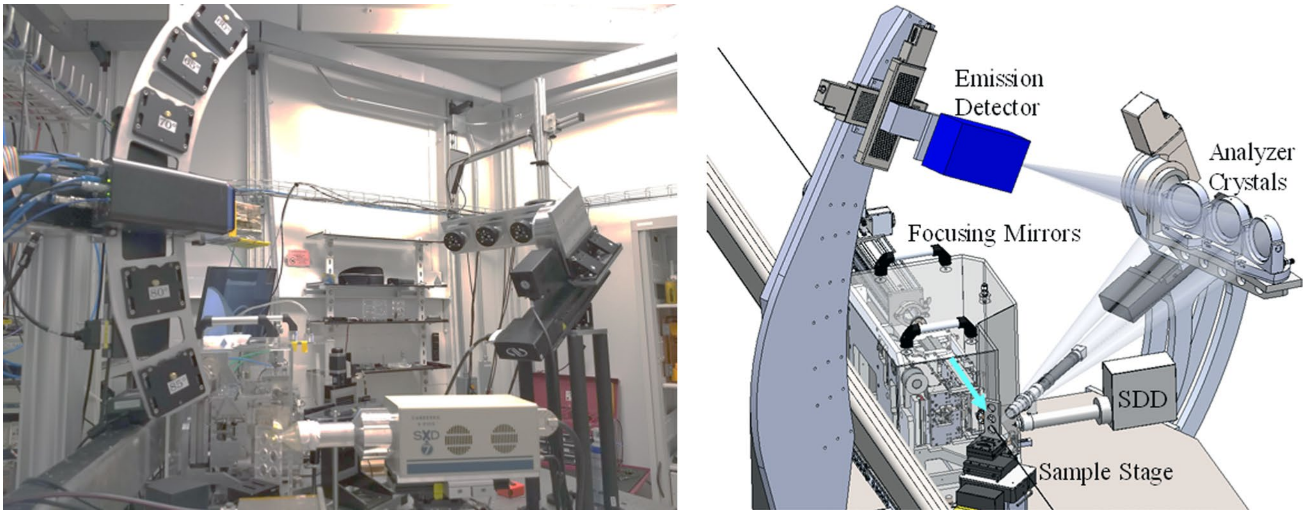

Fig. 11 X-ray microprobe apparatus in station 13-ID-E used for microbeam XRF, XAFS, and XRD. Left is a photograph of the setup and right is a schematic showing the availability of both energy dispersive (silicon drift) and HERFD detectors. The HERFD detection system is configured on a 1-m Rowland circle

the adjustable opening of which provides a convenient way of controlling the horizontal source size. Microfocusing mirrors in a KB geometry on the experimental table produce focused X-ray beams in the 1–2 µm size range. The flux in this beam spot is typically in the 10^{12} ph/sec range, depending on energy. The microprobe typically operates in a "45°" geometry with the sample plane 45° to the microfocused incident beam, an optical video microscope along the sample surface normal, a fluorescence detector at 90° to the incident beam (within the horizontal plane of the synchrotron for polarization reasons), and either an area detector for XRD studies or an ion chamber downstream of the sample for measuring X-ray sample absorption. New developments include the addition of a high energy-resolution fluorescence detection (HERFD) which uses crystal analyzer spectrometers at high Bragg angle to measure fluorescence XAFS with high energy resolution—1 eV. Energy resolution is set by the analyzer, not natural energy width of core–hole (often > 5 eV) leading to improved background rejection, improved XAS spectral resolution, and sensitivity to elements with overlapping lines, e.g., Eu Lα on Mn Kα.

Science Areas: X-ray microprobe techniques are used for fundamental geochemical studies of the complex heterogeneous systems such as soils including redox reactions that occur during diffusion, the complex interplay between roots and soils in controlling the sequestration of metals, the chemical nature of hydrothermal fluids and melts as recorded by fluid and melt inclusions in minerals, development of oxygen barometers for igneous materials, and compositions of extraterrestrial materials. Element-specific tomographic imaging techniques are used to study the chemical properties of systems during reactions, diffusion, and fluid transport. Science areas include the following:

Chemistry of magmas and their associated hydrothermal fluids. Microfocused X-ray absorption fine structure techniques allow for direct measurement of the speciation of redox sensitive elements (Fe, V, Cr, Eu, Ti, S, etc.) in magmatic minerals and glasses (Dyar et al. 2016; Cottrell et al. 2018; Head et al. 2018; Lanzirotti et al. 2018; Sutton et al. 2020b). Such direct measurement of elemental speciation and valence allows researchers to then quantitatively constrain the redox conditions for magmas derived by the melting of planetary mantles. This is critical to our understanding of the genesis and differentiation of magmas, associated ore deposits and for modeling the evolution of planetary interiors. As an example, Fig. 12 shows the fO_2 of least degassed magmas inferred from XANES analyses of melt inclusions in Reunion Island lavas (Brounce et al. 2022). These XAFS-based oxybarometric approaches rely on the sensitivity of XAFS to changes in the chemical speciation of redox-sensitive elements in igneous minerals and/or glasses in response to changing magmatic fO_2. The relationship between observed XAFS spectral features and oxygen fugacity can be established through development of system-specific calibration models (Sutton et al. 2020b).

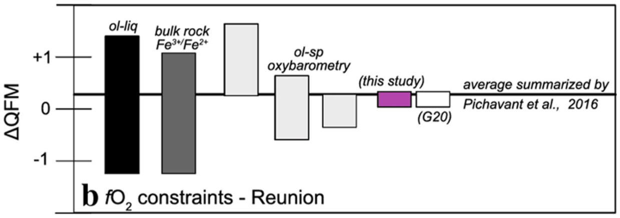

Fig. 12 Summary of the ranges of fO_2 inferred for Reunion Island lavas (Brounce et al. 2022).This plot is constructed after (Pichavant et al. 2016), with olivine-liquid equilibrium constraints from Boivin and Bachèlery (2009), bulk rock FeO and Fe_2O_3 analyses from Burgisser et al. (2015), and olivine-spinel equilibria from Burgisser et al. (2015) and Bureau et al. (1998). The solid black line demonstrates the likely fO_2 of Reunion magmas during petrogenesis summarized by Pichavant et al. (2016). The pink box marked "this study" shows the fO_2 of least degassed magmas inferred from XANES analyses of melt inclusions. It was concluded that the fO_2 of the mantle source of these Reunion lavas is lower than of the mantle sources of primitive, undegassed magmas from Hawaii, Iceland, the Canary Islands, and Mt. Erebus, and indistinguishable from that of the Indian-ocean upper mantle. This finding is consistent with previous suggestions that the source of Reunion lavas (and the C/FOZO/PREMA mantle component) contains little or no recycled materials and with the suggestion that recycled oxidized materials contribute to the high fO_2 of some other OIBs, especially those from incompatible-element-enriched mantle sources

Biogeochemistry. An important aspect of the research at GSECARS is to improve our understanding of the molecular-scale processes that control contaminant-microbe adsorption and redox reactions, and the effect of these processes on contaminant transport. The GSECARS microprobe provides instrumentation to biogeochemists for measuring redox mediated changes in chemistry (from the S K-edge through to the Cd K-edge) at appropriate length scales, both in natural samples and within environmentally controlled experimental cells (Cron et al. 2020; Phillips-Lander et al. 2020).

Cosmochemical studies of extraterrestrial materials. Clues to the origin and evolution of our Solar System and other cosmological bodies are locked within extraterrestrial materials available for laboratory study including lunar samples returned by the Apollo program; meteorites from the Moon, Mars and asteroids; interplanetary dust particles collected in the stratosphere; comet particles collected by the Stardust spacecraft; and solar wind collected by the Genesis spacecraft. FIB sectioning is being used to prepare monomineralic specimens for analysis (Sutton et al. 2020a). X-ray microprobe techniques provide a means to define the chemical states of these samples and obtain insight into the properties of their parent bodies.

Microtomographic imaging

Stations: 13-BM-D, 13-ID-E.

Techniques: Transmission, phase-contrast, differential absorption, and fluorescence computed microtomography

Technical description: GSECARS has three distinct but collaborating tomography programs. One is high-pressure tomography in a rotational Drickamer device in the 250 ton press in 13-BM-D. This GSECARS development, inspired by the ambient microtomography program, was the first high-pressure microtomography system in the world (Wang et al. 2005; Yu et al. 2019b). This system employs a thrust bearing to allow unlimited rotation under loads up to 50 tons. It is capable of pressures up to 12 GPa when using cupped Drickamer anvils; a maximum temperature of 2200 K can be obtained. The second program involves X-ray fluorescence tomography which is conducted using a focused undulator beam in the 13-ID-E microprobe station. The third program is the absorption tomography program conducted at ambient or relatively low pressures in 13-BM-D (Rivers et al. 1999, 2010; Rivers and Wang 2006; Rivers 2012, 2016).

The unique detection system for the absorption tomography apparatus (Fig. 13) consists of a single-crystal scintillator (converts X-rays to visible light), a microscope objective (magnifies the scintillator image), and a 1920 × 1200 pixel fast CMOS camera. Three modes can be used. *Monochromatic beam mode* uses a high-resolution Si (111) double-crystal monochromator capable of operating with fixed offset in the energy range 10–80 keV with a very narrow (~0.01%) energy bandwidth (element-specific applications, such as "above-edge, below-edge" subtraction imaging). Pink beam mode provides more than 1000 times brighter (photons/s/0.1% bandwidth/mrad^2) than the monochromatic mode, and thus allows much faster data collection. The water-cooled, vertically downward deflecting, 1.1 m long, Pt-coated mirror in the 13-BM-B station can be dynamically bent to either a concave (focusing) or convex (defocusing) shape. High-energy X-rays are removed by the adjustable mirror cutoff energy and water-cooled absorption filters are used to remove low energy X-rays. White beam mode uses neither the monochromator nor the mirror and so provides the highest flux and the highest energy X-ray spectrum, at the expense of vertical beam size. In the high-pressure tomography apparatus, pressure is monitored using energy-dispersive powder diffraction. The monochromator and mirror systems allow fast switching between either monochromatic or pink mode for imaging and white beam mode for diffraction. New developments include sample stage improvements to allow loads greater than 25 kg offering opportunities to employ much more complex sample environments. Construction is in progress of a triaxial deformation cell capable of confining pressures up to 100 MPa, axial loads to 200 MPa, while maintaining fluid flow and temperatures up to 500 K.

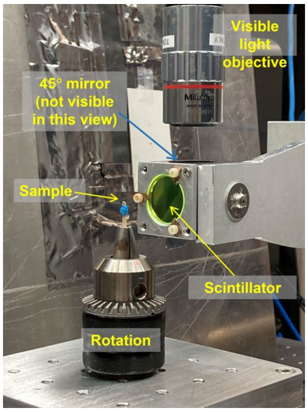

Fig. 13 Computed microtomography apparatus in station 13-BM-D used for transmission, phase-contrast, and differential absorption tomography. The X-ray beam enters on the left and the sample-transmitted image is converted to visible light by a single-crystal scintillator. A 45° mirror (not visible in this view) directs the image to a magnifying microscope objective. This image is then captured by a 1920 × 1200 pixel fast CMOS camera (out of view at top)

Science areas: Tomographic imaging techniques are used to study the internal microstructures of complex materials. The LVP tomography apparatus can be also used for studies of equations of state of liquids and amorphous materials at high pressure (Lesher et al. 2009). By twisting the opposed anvils, this apparatus can be used for large shear deformation combined with 3D texture imaging. This combination has been used to study liquid FeS melt in solid olivine matrix, to understand segregation process of metallic melts as a mechanism for the formation of the Earth's core (Todd et al. 2016). In multi-phase solids, this combination has been used to understand texture-induced rheological property changes (Wang et al. 2011). It has also been used for some lower pressure studies for example proppants employed in the oil industry (Sanematsu et al. 2015). The X-ray fluorescence tomography apparatus can be used to reconstruct element-specific virtual cross sections in small samples, for example Mn and Fe distributions in genetically modified seeds (Socha and Guerinot 2014) and plants (Chu et al. 2017). The absorption tomography system can be used for the study of the internal structures of precious samples such as fossils, the distribution and location of inclusions in diamonds, the porosity and density of weathered rocks, studies of granular flow, and the transport of fluids such as water and oils in porous media.

Flow dynamics of fluids and solids. Many processes in the Earth's surface are controlled by the microscale interaction of water and air with the solid phase (soils, sediments, rock) in pore spaces within the subsurface. The distribution in time and space of fluids in pores ultimately controls subsurface flow and transport processes relevant to groundwater resource management and remediation as well as oil and gas exploration and recovery. Many of the mechanisms operating at the microscale can be observed through the measurement of relevant physical parameters (e.g. fluid phase content and distribution, pore size distribution, permeability, porosity) using computed microtomography. In addition, the flow of solids (rheology) is important in understanding earthquake propagation.

Enhancing residual trapping of supercritical CO_2 via cyclic injections. Synchrotron X-ray tomographic imaging was used to investigate the pore-scale characteristics and residual trapping of supercritical CO_2 ($scCO_2$) over the course of multiple drainage-imbibition (D-I) cycles in Bentheimer sandstone cores (Herring et al. 2016). The hysteretic pore-scale behavior of the $scCO_2$-brine-sandstone system (Fig. 14) suggested that cyclic multi-phase flow could potentially be used to increase $scCO_2$ trapping for sequestration applications.

Solute mixing regulates heterogeneity of mineral precipitation in porous media. Synchrotron X-ray microtomography was used to track the spatio-temporal evolution of mineral precipitation and the consequent alteration of the pore structure (Cil et al. 2017). Column experiments were conducted by injecting $CaCl_2$ and $NaHCO_3$ solutions into granular porous media either as a premixed supersaturated solution (external mixing) or as separate solutions that mixed within the specimen (internal mixing). The similar pore-scale evolution patterns suggest that the clogging of individual pores

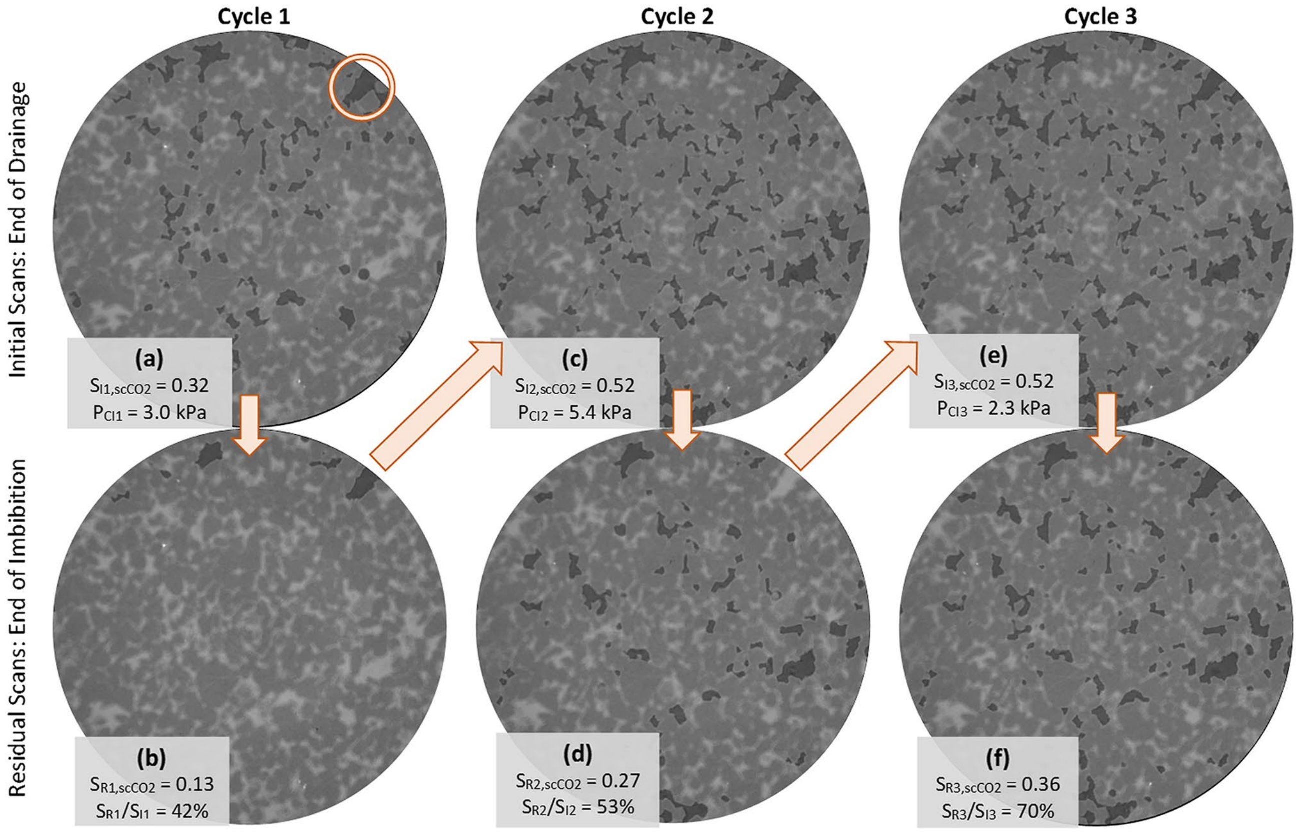

Fig. 14 A cross-sectional tomographic slice of grayscale data over the course of three drainage-imbibition (D-I) cycles in Bentheimer sandstone cores (Herring et al. 2016). Highly attenuating 1.0 M KI brine presents as light gray, the sandstone grains appear to be moderate gray, and the lower attenuating supercritical CO_2 ($scCO_2$) phase is identified by the dark gray (**a**, **c**, and **e**). The core at the end of drainage ("initial state") and (**b**, **d**, and **f**) the same core at the end of the subsequent imbibition ("residual state"); the cycle number (*i*) increases from left to right. For the initial states, the $scCO_2$ saturation ($S_{Ii,scCO2}$) and drainage endpoint capillary pressure (P_C) are given; For residual states, $scCO_2$ saturation ($S_{Ri,scCO2}$) and trapping efficiency (S_{Ri}/S_{Ii}) are given. The first D-I cycle (**a** and **b**) results in relatively low residual trapping; after the second cycle (**c** and **d**) residual trapping and trapping efficiency increases; and the third cycle (**e** and **f**) results in the highest values for $scCO_2$ trapping and trapping efficiency

depends primarily on local supersaturation state and pore geometry.

Effect of pore morphology on microbial enhanced oil recovery: X-ray computed microtomography was utilized to characterize the pore morphologies and analyze residual oil blob mobilization during simulated microbial enhanced oil recovery (MEOR; (Armstrong et al. 2015). Results demonstrated that bioclogging with interfacial tension reduction is the most effective MEOR treatment option in terms of additional oil recovered (AOR) for the pore morphologies with the smallest pore throat radii and that AOR increases with increasing pore body and throat radii, as well as pore sphericity.

Protection of soil carbon within macro-aggregates depends on intra-aggregate pore characteristics. CO_2 respiration measurements of intact soil samples combined with X-ray computed micro-tomography imaging was used to investigate how micro-environmental conditions, represented by soil pores, influence decomposition of particulate organic matter (POM; (Kravchenko et al. 2015). Atmosphere-connected soil pores were found to influence soil carbons, and especially POMs, decomposition. It was demonstrated that the presence of a feed-forward relationship between soil C decomposition and pore connections enhances it.

Technical synergy

The availability of multiple, Earth science relevant instruments in one facility naturally leads to synergy in terms of technical developments. At the first level, this means there exists a pool of equipment to be shared by multiple instruments. This multi-tasking, as well as staff sharing, translates into major economies of scale. It also means that new hybrid instrumentation is developed through collaborations of specialists with expertise in different methods. Some of these synergies are described below.

X-ray optics: Several hardware devices developed at GSECARS have found worldwide use. These include a pair of very asymmetric, elliptical, Kirkpatrick-Baez mirrors developed by Peter Eng that focuses the APS source to a few microns (Eng et al. 1998). At GSECARS, these mirrors are used by the X-ray microprobe and DAC instruments. Large, water-cooled Kirkpatrick-Baez mirrors designed by Peter Eng are in use at GSECARS on all four beamlines, for example for the vertical focusing for diamond anvil cell experiments on 13-BM-C and 13-BM-D, for defocusing for pink beam tomography on 13-BM-D, and for both horizontal and vertical focusing at the rotation center of the diffractometer in 13-ID-C.

High-pressure Tomography: High-pressure tomography was developed by GSECARS as a synergy between the ambient tomography and LVP programs. The development of a rotational Drickamer device in a 250 ton press was the first high-pressure microtomography system in the world (Wang et al. 2005; Yu et al. 2019b) and has been used for studies of viscous liquids and amorphous materials at high pressure (Xu et al. 2020b).

Detectors: A suite of state-of-the-art X-ray detectors nominally dedicated to a particular instrument but available to be shared among the experimental stations including the following with information on their primary use:

- *Pilatus3 X CdTe 1 M* array detector (981 × 1043 pixels). High pressure diffraction in diamond anvil cell in 13-ID-D. Up to 500 frames/s. Shared with sector 15, ChemMatCARS
- *Pilatus3 X CdTe 300 K-W* array detector (1475 × 195 pixels). Amorphous diffraction in Paris-Edinburgh press and diamond anvil cells with Soller slits in 13-ID-C.
- *Pilatus3 S 1 M* array detector (981 × 1043 pixels) with 1 mm silicon sensor. Jointly funded with COMPRES for PX^2 program at 13-BM-C for high-pressure diffraction in the DAC as well as ambient-pressure diffraction.
- *Pilatus3 S 1 M CdTe* array detector (981 × 1043 pixels) for DAC, LVP, and mineral inclusion X-ray diffraction in 13-BM-D.
- *Pilatus 100 K* array detectors with collimating flight paths for interface scattering studies in 13-ID-C and 13-BM-C
- *Dectris Eiger 500 K* array detector with 450 µm silicon sensor. For diffraction mapping and HERFD with the 13-ID-E microprobe
- *Dectris Eiger2 S 1 M* array detector (1028 × 1062 pixels). For diffraction mapping and HERFD on 13-ID-E microprobe
- *Hitachi Vortex ME4* silicon drift, energy dispersive spectrometers; two are available. For energy dispersive measurements with the 13-ID-E microprobe and 13-ID-C diffractometer
- *Mirion 7-element X-PIPS* silicon drift, energy dispersive spectrometer. For energy dispersive measurements with the 13-ID-E microprobe
- *MAR165 CCD large area detector (2048 × 2048 pixels)* for DAC, LVP and mineral inclusion X-ray diffraction in 13-ID-D, 13-BM-C and 13-BM-D.

Gas-loading Facility: GSECARS (with support from COMPRES) developed a gas-loading system for diamond anvil cells at the APS (Rivers et al. 2008), which is used by experimenters at 13-ID-D, 13-BM-D, and 13-BM-C as well as many other APS beamlines (Fig. 15). In addition, a mail-in service is provided for users who will be running experiments at locations other than the APS.

Software: GSECARS has developed advanced software that is required for the needs of all GSECARS beamlines, but also benefits the larger scientific community, M. Rivers has collaborated with other groups at the APS in the development of EPICS, a control and data acquisition system for accelerators and beamlines. A major portion of this software is for collecting data from advanced detectors and cameras. Matt Newville has developed two software packages that are widely used around the world. One is Python language support for EPICS (http://cars.uchicago.edu/software/python/pyepics3), and the other is XAFS analysis software (http://cars.uchicago.edu/ifeffit, http://cars.uchicago.edu/xraylarch). *Dioptas* is a Python-based program for on-the-fly data processing and exploration of two-dimensional X-ray diffraction area detector data, specifically designed for the large amount of data collected at XRD beamlines at synchrotrons (Prescher and Prakapenka 2015). It is used to process diffraction data from beamlines around the world, including the DAC and X-ray microprobe (XRM) stations at GSECARS.

Fig. 15 The GSECARS and COMPRES jointly funded gas-loading system for diamond anvil cells located adjacent to experimental station 13-ID-D. The system can load many kinds of diamond anvil cells with a closure mechanism using motor driven screws which close a clamping device, not the cell itself. This design makes it easy to pressurize new cell designs using a different clamp or different spacer. The system has optical access for sample viewing and online ruby fluorescence pressure measurement. 1 = Microscopy and ruby fluorescence system; 2 = Pneumatic cylinder; 3 = Pressure vessel; 4 = Diamond anvil cell clamp; 5 = Vessel bottom plug; 6 = Gas supply tank (He, N_2, Ne, Ar, Xe, or CO_2); 7 = Pressure gages; 8 = Control panel; 9 = Emergency stop button; 10 = Gear boxes for various DACs; 11 = High pressure valves; 12 = Compressor

Science synergy

The availability of multiple, Earth science relevant instruments in one facility also leads to synergy in scientific projects. Typically, this means a particular science problem is tackled either with multiple instruments and techniques at the sector (e.g., X-ray microprobe and diffraction in the DAC), or addressed using synergistically developed instrumentation (e.g., tomography cell for the large volume press). Importantly, beamline scientists with varied expertise are immediately available to provide assistance and collaborate on such problem-solving. Examples of science projects carried out synergistically between different experimental stations are described below.

Diamond inclusions: A notable example is the work of Wenz and co-workers studying inclusions in diamonds (Wenz et al. 2019). A fast, high-throughput method for micromineral inclusion identification has been developed by first collecting microtomography images in station 13-BM-D (Fig. 16) and then converting the geometry to the six-circle single-crystal diffractometer in station 13-BM-C using a portable radiography setup and then collecting X-ray diffraction data on the identified inclusions in 13-BM-C. In addition, some inclusions have been analyzed for cation valence using

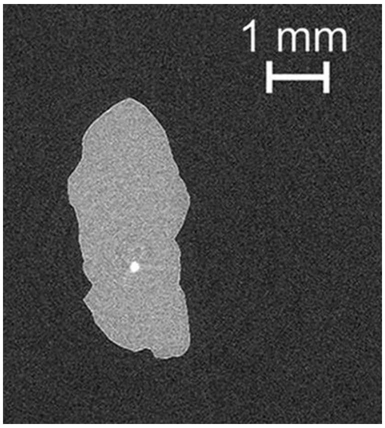

Fig. 16 Tomographic slice of diamond 6b_09 (light gray region) with a high-absorbing goethite (FeOOH) inclusion (small bright spot) (from Wenz et al. 2019)

XANES on the XRM in 13-ID-E, to help identify color centers. Another application using high-pressure X-ray diffraction at 13-ID-D and XRF mapping at 13-ID-E was the work of Tschauner and co-workers (Tschauner et al. 2018) who showed that ice-VII (Fig. 17) occurs as inclusions in natural diamond and serves as an indicator for water-rich regions in Earth's mantle, notably in the upper transition zone and the 660-km boundary region. Such regions are suspected to play a key role in the global water budget and the mobility of heat-generating elements.

Structural behavior of deep Earth analogs: The DAC has been combined with extended X-ray absorption fine structure (EXAFS) methods to study the structural behavior of germanium dioxide (GeO_2) glass (Hong et al. 2013; Hong and Newville 2020). GeO_2 is considered a chemical and structural analog of silica (SiO_2) displaying similar compression behavior but at lower pressures. The difference between the nearest Ge–O distances of glassy and rutile-type GeO_2 disappears at the Ge–O distance maximum at 20 GPa, indicating completion of the tetrahedral–octahedral transition in GeO_2 glass. Above 40 GPa, GeO_2 forms a dense octahedral glass and there is spectral evidence for subtle changes in the dense glass continuing to occur at these high pressures. A pyrite-type local structural model for the glass can provide a reasonable fitting to the XAFS spectra at 64 GPa.

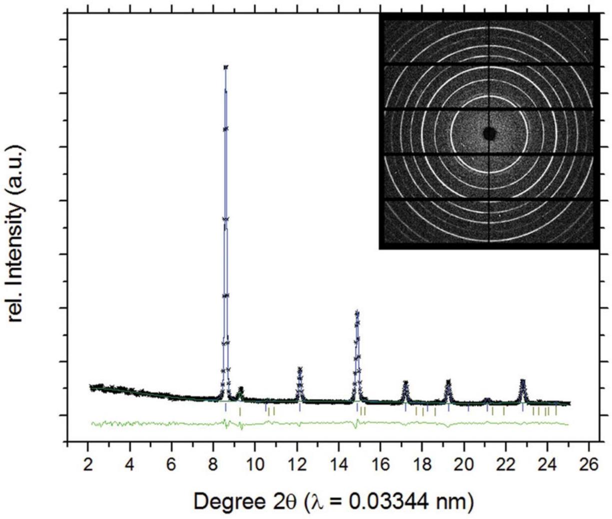

Fig. 17 X-ray diffraction pattern of ice-VII in diamond M57666 from Orapa. Black crosses are data points; the Rietveld refinement (blue curve), and residual fit (green curve). The equation of state allows estimation of the current pressure of this inclusion of ice-VII as 9.2 ± 1.6 GPa. The inset is a diffraction image of ice-VII (From Tschauner et al. 2018)

Shear deformation in metal-silicate composites: These experiments rely on the unique tomographic capability of the multi-anvil press which allows additional shear stress to be applied to a sample that is under uniaxial load. Shear-induced iron silicate segregation can be studied in situ at high pressure and high temperature to help understand the mechanism of the Earth's core formation (Todd et al. 2016). In this study, samples consisting of San Carlos olivine and 4.5 vol % FeS were heated (1370 K) at 1.5 GPa, conditions under which FeS is liquid and olivine is solid. A shear stress is then applied in the horizontal plane by rotating the top and bottom Drickamer anvils in opposite directions. Melt pockets change their shapes, sizes, and connectivity at various shearing levels (Fig. 18). The duration of each deformation step was ~1 h. Permeability simulations were performed on the 3D tomography images to determine the effect of shear deformation on connectivity and permeability within the sample.

Elasticity of Fe-enriched diopside at high pressure: High resolution X-ray diffraction and Brillouin spectroscopy can be collected simultaneously from the same sample area and in the same pressure–temperature environment in station 13-BM-D. This unique system (Fig. 3) makes it possible to measure sound velocities and densities of materials simultaneously, resulting in an absolute pressure scale and determinations of important material properties (e.g., equations of state and elasticity) as a function of pressure and temperature. In one study (Fig. 19), the single-crystal elasticity of Fe-enriched diopside ($Di_{80}Hd_{20}$, Di-diopside, and Hd-hedenbergite; also called Fe-enriched clinopyroxene) at high-pressure conditions up to 18.5 GPa was measured (Fan et al. 2020). The results were used in evaluating the effects of pressure and Fe substitution on the full single-crystal elastic moduli across the Di-Hd solid-solution series to better understand the seismic velocity profiles of the upper mantle. The presence of Fe-enriched pyroxenite was suggested to be an effective mechanism to cause low-velocity anomalies in the upper mantle regions atop the 410 km discontinuity under cold subducted slab conditions.

Oxybarometry method for high-pressure environments in the DAC: XANES methods developed on the XRM for oxybarometry of igneous Earth and planetary materials (Sutton et al. 2005; Lanzirotti et al. 2018) were adapted in developing an approach to use *V* valence in sensor glass fragments as a proxy for DAC redox environments. The idea is to include well-characterized glass fragments within the DAC and laser melt these at times when redox condition determinations are desired. When the glass melts, the *V* valence is re-equilibrated depending on the surrounding fO_2 and fast quenching freezes-in that valence state for subsequent ex-situ analysis. Only proof-of-concept measurements have

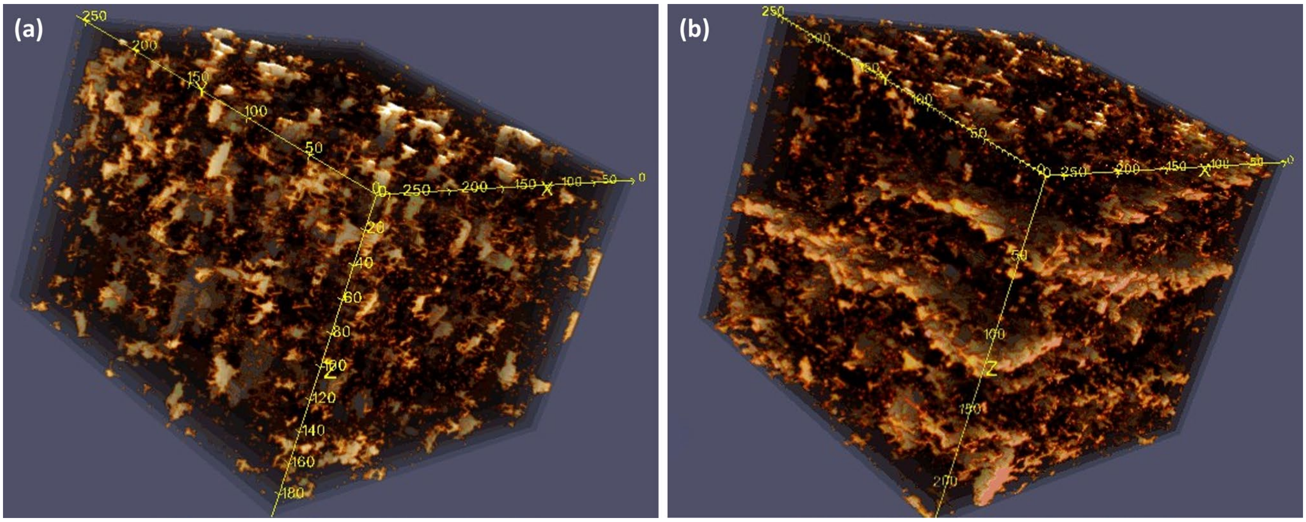

Fig. 18 X-ray tomographic image (after binarization) of olivine/FeS assemblage under shear stress in the LVP. Left: before large shear deformation, showing individual FeS blobs (orange) in olivine matrix (dark brown). Right: after large shear deformation, showing the formation banded structure of FeS melts. Images courtesy of H. Watson and K. Todd from the study described in Todd et al. (2016)

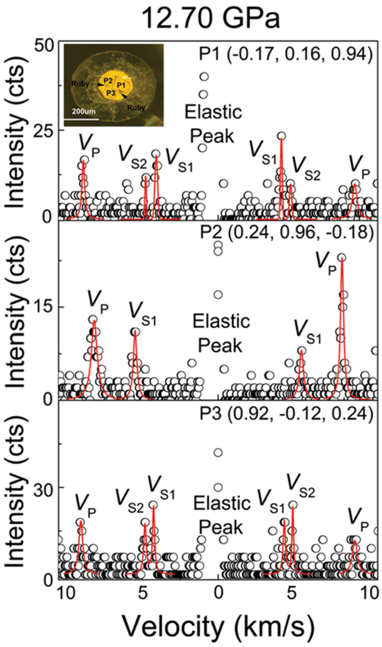

Fig. 19 Representative Brillouin spectra of single-crystal $Di_{80}Hd_{20}$ at 12.70 GPa. Open circles = experimental data; solid lines = fitted V_P and V_S peaks. The inset is a representative photo of the three crystal platelets in the sample chamber at 12.70 GPa and 300 K (From Fan et al. 2020)

been conducted to date and further development work is needed on this method.

Acoustic emission in LVP: Acoustic emission has been interfaced with the two deformation DIA apparatus in both 13-BM-D and 13-ID-D to investigate failure mechanisms in rocks undergoing phase transformations and metamorphic reactions (Schubnel et al. 2013). Pressures up to 10 GPa have been reached, with successful AE detection and location. Brittle deformation in the D-DIA coupled with acoustic emission monitoring has enabled systematic laboratory simulations on possible mechanisms triggering deep earthquakes between ~50 km and 700 km. Studies have been conducted of systems involving dehydration (antigorite, partially serpentinized olivine, and glaucophane-blueschist facies rocks) (Ferrand et al. 2017; Gasc et al. 2017; Incel et al. 2017), metamorphic reactions (granulite to eclogite) (Shi et al. 2018; Incel et al. 2019), and the olivine-spinel phase transformation (Schubnel et al. 2013; Wang et al. 2017).

User program including access procedure

All available user operations beam time at GSECARS is allocated through the APS General User Program and all GSECARS users must submit access proposals to this system. Useful links are provided here. Beam time is allocated three times per year.

GSECARS “Quick Guide for New Users” is here: https://gsecars.uchicago.edu/user-resources/.

APS user information is here: https://www.aps.anl.gov/Users-Information.

Apply for beam time here: https://www.aps.anl.gov/Users-Information/About-Proposals/Apply-for-Time.

Submission deadlines are here: https://www.aps.anl.gov/Users-Information/About-Proposals/Proposal-Deadlines-and-Meetings.

For assistance in submitting proposals, contact one of the GSECARS beamline scientists listed on the Quick Guide page shown above.

General User Proposals are peer reviewed and rated by a technique-specific Proposal Review Panel (PRP). Beam time is awarded based on score and feasibility. Users may select more than one beamline when submitting a proposal to increase the chances of receiving beam time. Proposals expire in 2 years or when the number of PRP recommended shifts has been used, whichever comes first. An aging process is in place which improves a proposal's rating when unsuccessful for a maximum of two times. The APS Beamtime Allocation Committee (BAC) allocates 25% of the available time. GSECARS allocates the remaining 75% based largely on ratings from the APS PRPs and Earth science relevance.

The GSECARS sector is oversubscribed; there are more requests for beam time than can be handled. This oversubscription is managed by limiting the number of days each experiment receives, rejecting experiments, and referring experiments to other suitable synchrotron facilities. The challenge has been to balance the desire to give beam time to as many highly rated proposals as possible while providing sufficient beam time to each experiment to accomplish the intended goals. The proposal success rate is ~ 60% in a typical cycle.

GSECARS users come from all over the world. Recent statistics showed 76% were from the USA, 11% from Europe, 7% from Canada, and 6% from Asia and Australia. 83% of the investigators were affiliated with universities; 6% with government laboratories (e.g., national laboratories); 1% with other government agencies (e.g., USGS, EPA); 9% with private institutions (e.g., Carnegie Institution of Washington); and 1% with industry. GSECARS staff work with users through the entire process including submission of beam time proposals, design of experiments, preparation of samples, collection of data, analysis and interpretation of the data, and preparation of publications. Most publications resulting from work at GSECARS include one or more GSECARS beamline scientists as co-authors. Publications are included in the APS Publication Database (https://gsecars.uchicago.edu/funding-and-publications). About 60% of the GSECARS users are students or postdocs at universities and colleges.

Management

GSECARS management consists of two Project Managers: Mark Rivers and Stephen Sutton and six Technical Groups organized around the six principal techniques in the sector. Senior GSECARS staff members serve as leaders of these groups as shown below:

- Diamond Anvil Cell (Vitali Prakapenka, Research Professor)
- Large-Volume Press (Yanbin Wang, Research Professor)
- Microtomography (Mark Rivers, Research Professor)
- X-ray Absorption Fine Structure Spectroscopy (Matthew Newville, Research Professor)
- X-ray Diffraction and Scattering (Peter Eng, Research Professor; Joanne Stubbs, Associate Research Professor)
- X-ray Fluorescence Microprobe (Stephen Sutton, Antonio Lanzirotti, Matt Newville, Research Professors)

These individuals have the responsibility to lead the development of science, instrumentation and user community in their particular area. In addition, the leaders work closely with users to ensure the success of experiments (experiment design, experiment conduct, data analysis, etc.) and receive input from them on potential new technical directions. This management configuration has worked successfully throughout the > 20-year history of GSECARS.

Anticipated advances with APS upgrade

The Advanced Photon Source is planning a major upgrade to replace the entire accelerator with a new Multi-Bend Achromat (MBA) design. This upgrade will reduce the horizontal electron beam size and divergence, resulting in ~ 100-fold increase in the X-ray brightness and coherence. The upgrade will include reducing the machine energy from 7 to 6 GeV, which necessitates replacing all of the undulators with ones with shorter periods to cover the same energy range. The increased brightness of the APS upgrade (APS-U) will allow dramatic increases in the X-ray flux that can be delivered into a given size focal spot (~100X) or provide the same flux that is available now into a much smaller focal spot (~10X smaller). These improvements will allow fundamentally new types of studies. Several anticipated advances are highlighted here.

High pressure science: The pressure–temperature conditions required to understand the nature and origin of different planetary systems are either very difficult to reach (Earth's core-mantle boundary and core, > 130 GPa and > 4000 K) or lay beyond typical experimental limits (gas giants and exoplanets, > 400 GPa and > 6000 K). Double stage anvil techniques and toroid-shaped anvils have the potential for studying materials in situ at high temperatures and multi-megabars pressures (Dubrovinskaia et al. 2016). APS-U will provide greater flux into a smaller spot, 300 nm, greatly enhancing in-situ XRD high-pressure studies in the DAC. APS-U and associated beamline enhancements will also advance multi-phase experiments with both DAC and multi-anvil press high-PT devices in station 13-ID-D. APS-U will improve the capabilities for producing the tightly collimated X-ray beams required to minimize contamination from the surrounding solid pressure media for structure and composition determinations. In deformation experiments in the press for rheology studies, APS-U will provide the required high brightness, monochromatic source with energies up to 80 keV, thus allowing useable d-spacing to be "compressed" within the limited solid angle of 6–7 degrees.

Microspectroscopy: APS-U will allow improvements in the spatial resolution (to the sub-micron regime) and sensitivity of the XRM thereby advancing studies of minute and fine-grained specimens. An example is valence state μXAFS measurements of sub-micron mineral phases in early solar system materials to infer the oxidation states of the environments from which they formed. Environmental science problems also will take advantage of the new capabilities in seeking to understand the biogeochemical controls on the heterogeneous reactivity of elements at mineral-fluid interfaces. There are also new opportunities for understanding controls on chemical incorporation in colloids, on atmospheric particles, and within micro-organisms. Some of the most abundant marine organisms in tropical and sub-tropical oceans, whose activity is known to impact oceanic and atmospheric elemental cycles, are at the scale of 500 nm, too small to be effectively analyzed with current capabilities. The causes and treatment of respiratory diseases associated with the inhalation of fine particulate matter is another research area of potentially high societal impact.

Interface science: The 13-ID-C interface science program will expand the suite of accessible minerals and make coherent scattering methods such as Bragg Coherent Diffractive Imaging (BCDI) feasible. 13-ID-C currently offers two primary classes of techniques: (1) surface and interface scattering (both resonant and non-resonant) such as crystal truncation rod diffraction and resonant anomalous X-ray reflectivity to determine atomic-level interfacial structures and adsorbate positions; and (2) Grazing incidence (GI) methods including GI-XAS and long-period standing wave fluorescence yield which are laterally averaged but have inherent nanometer-scale resolution in the surface-normal dimension. Experiments in the first class require multi-axis diffractometry and have been limited to single crystals ~ millimeters in lateral extent The technique will have far more scientific impact when the proposed enhancements allow applications to smaller crystals, where size is often a limiting factor for many important minerals. The second (GI) class of techniques will also benefit from diffractometer upgrades. Coherent scattering techniques will enable the investigation nanoparticle strain and morphology including the effects of solution chemistry, reaction dynamics, and heterogeneous systems that cannot be currently investigated.

Summary

GSECARS is a comprehensive analytical laboratory for Earth and environmental science research. State-of-the-art instruments are available for most X-ray-based analytical techniques in demand by Earth and environmental scientists including (1) high-pressure/high-temperature diffraction, scattering, and spectroscopy using the laser heated diamond anvil cell; (2) high-pressure/high-temperature diffraction, scattering, and imaging using the large-volume press; (3) powder, single crystal and interface diffraction; (4) X-ray absorption fine structure spectroscopy; (5) X-ray fluorescence microprobe analysis; and (6) microtomography. Senior level staff are available at each instrument to collaborate on all aspects of the analytical work including experiment design, sample preparation, data collection, data interpretation, and publication preparation. The intimate association of the various techniques leads to synergistic developments in instrumentation, analytical capabilities, and scientific projects. A suite of state-of-the-art X-ray instrumentation designed and build in-house, including custom X-ray optics, specialized sample environments and positioning systems, as well as pixel-array and multi-crystal energy dispersive detectors, are available to be shared among the experimental stations.

Acknowledgements GeoSoilEnviroCARS is primarily supported by the National Science Foundation—Earth Sciences Instrumentation and Facilities (EAR-1634415). Some support also derives from development grants from other NSF agencies (Geophysics-EAR-1620548, Petrology and Geochemistry- EAR-1834930, CSEDI-EAR-1661489, FRES-EAR-1925920), DOE-BES Geosciences (DE-SC0019108, DE-SC0020112, DE-SC0021222), NASA (LARS-80NSSC21K0611, ANGSA-80NSSC19K0802 subaward, SSERVI-80NSSC19M0215 subaward). GSECARS uses resources of the Advanced Photon Source, a U.S. Department of Energy (DOE) Office of Science User Facility operated for the DOE Office of Science by Argonne National Laboratory under Contract No. DE-AC02-06CH11357.

Funding National Science Foundation, EAR-1634415, Mark L. Rivers, U.S. Department of Energy, DE-SC0019108, Joanne E. Stubbs, DE-SC0020112, Mark L. Rivers, DE-SC0021222, Matthew Newville, National Aeronautics and Space Administration, 80NSSC21K0611, Stephen R. Sutton.

References

Armstrong RT, Wildenschild D, Bay BK (2015) The effect of pore morphology on microbial enhanced oil recovery. J Petrol Sci Eng 130:16–25

Boivin P, Bachèlery P (2009) Petrology of 1977 to 1998 eruptions of Piton de la Fournaise, La Réunion Island. J Volcanol Geoth Res 184:109–125

Bracco JN, Lee SS, Stubbs JE et al (2017) Hydration structure of the barite (001)–water interface: comparison of x-ray reflectivity with molecular dynamics simulations. J Phys Chem C 121:12236–12248

Bracco JN, Lee SS, Stubbs JE et al (2018) Simultaneous adsorption and incorporation of Sr2+ at the barite (001)–water interface. J Phys Chem C 123:1194–1207

Brounce M, Stolper E, Eiler J (2022) The mantle source of basalts from Reunion Island is not more oxidized than the MORB source mantle. Contrib Miner Petrol 177:1–18

Bureau H, Métrich N, Pineau F, Semet M (1998) Magma–conduit interaction at Piton de la Fournaise volcano (Réunion Island): a melt and fluid inclusion study. J Volcanol Geoth Res 84:39–60

Burgisser A, Alletti M, Scaillet B (2015) Simulating the behavior of volatiles belonging to the C–O–H–S system in silicate melts under magmatic conditions with the software D-Compress. Comput Geosci 79:1–14

Chantel J, Frost DJ, McCammon CA et al (2012) Acoustic velocities of pure and iron-bearing magnesium silicate perovskite measured to 25 GPa and 1200 K. Geophys Res Lett 39:19

Chantel J, Manthilake G, Andrault D et al (2016) Experimental evidence supports mantle partial melting in the asthenosphere. Sci Adv 2:e1600246

Chariton S, Bykov M, Bykova E et al (2020) The crystal structures of Fe-bearing MgCO3 sp2- and sp3-carbonates at 98 GPa from single-crystal X-ray diffraction using synchrotron radiation. Acta Crystallographica Section E 76:715–719

Chen H, Leinenweber K, Prakapenka V et al (2020a) Possible H_2O storage in the crystal structure of $CaSiO_3$ perovskite. Phys Earth Planet Inter 299:7. https://doi.org/10.1016/j.pepi.2019.106412

Chen HW, Leinenweber K, Prakapenka V et al (2020b) Phase transformation of hydrous ringwoodite to the lower-mantle phases and the formation of dense hydrous silica. Am Miner 105:1342–1348. https://doi.org/10.2138/am-2020-7261

Chen HW, Xie SY, Ko B et al (2020c) A new hydrous iron oxide phase stable at mid-mantle pressures. Earth Planet Sci Lett 550:9. https://doi.org/10.1016/j.epsl.2020.116551

Chen SA, Heaney PJ, Post JE et al (2021) Superhydrous hematite and goethite: a potential water reservoir in the red dust of Mars? Geology 49:1343–1347

Chu H-H, Car S, Socha AL et al (2017) The Arabidopsis MTP8 transporter determines the localization of manganese and iron in seeds. Sci Rep 7:1–10

Cil MB, Xie M, Packman AI, Buscarnera G (2017) Solute mixing regulates heterogeneity of mineral precipitation in porous media. Geophys Res Lett 44:6658–6666

Cottrell E, Lanzirotti A, Mysen B et al (2018) A Mössbauer-based XANES calibration for hydrous basalt glasses reveals radiation-induced oxidation of Fe. Am Min: J Earth Planet Mater 103:489–501

Cron BR, Sheik CS, Kafantaris F-CA et al (2020) Dynamic biogeochemistry of the particulate sulfur pool in a buoyant deep-sea hydrothermal plume. ACS Earth Space Chem 4:168–182. https://doi.org/10.1021/acsearthspacechem.9b00214

Dera P, Zhuravlev K, Prakapenka V et al (2013) High pressure single-crystal micro X-ray diffraction analysis with GSE_ADA/RSV software. High Pressure Res 33:466–484. https://doi.org/10.1080/08957959.2013.806504

Desmau M, Gélabert A, Levard C et al (2018) Dynamics of silver nanoparticles at the solution/biofilm/mineral interface. Environ Sci Nano 5:2394–2405

Desmau M, Levard C, Vidal V et al (2020) How microbial biofilms impact the interactions of quantum dots with mineral surfaces? NanoImpact 19:100247

Dorfman SM, Badro J, Nabiei F et al (2018) Carbonate stability in the reduced lower mantle. Earth Planet Sci Lett 489:84–91. https://doi.org/10.1016/j.epsl.2018.02.035

Dubrovinskaia N, Dubrovinsky L, Solopova NA et al (2016) Terapascal static pressure generation with ultrahigh yield strength nanodiamond. Sci Adv 2:e1600341. https://doi.org/10.1126/sciadv.1600341

Dyar MD, McCanta M, Breves E et al (2016) Accurate predictions of iron redox state in silicate glasses:a multivariate approach using X-ray absorption spectroscopy. Am Miner 101:744–747

Eng PJ, Newville M, Rivers ML, Sutton SR (1998) Dynamically figured Kirkpatrick Baez X-ray microfocusing optics. In: X-Ray Microfocusing: Applications and Techniques. International Society for Optics and Photonics, pp 145–157

Fan DW, Fu SY, Yang J et al (2019) Elasticity of single-crystal periclase at high pressure and temperature: the effect of iron on the elasticity and seismic parameters of ferropericlase in the lower mantle. Am Miner 104:262–275. https://doi.org/10.2138/am-2019-6656

Fan D, Fu S, Lu C et al (2020) Elasticity of single-crystal Fe-enriched diopside at high-pressure conditions: implications for the origin of upper mantle low-velocity zones. Am Miner 105:363–374

Ferrand TP, Hilairet N, Incel S et al (2017) Dehydration-driven stress transfer triggers intermediate-depth earthquakes. Nat Commun 8:1–11

Fu SY, Yang J, Zhang YJ et al (2018) Melting behavior of the lower-mantle ferropericlase across the spin crossover: implication for the ultra-low velocity zones at the lowermost mantle. Earth Planet Sci Lett 503:1–9. https://doi.org/10.1016/j.epsl.2018.09.014

Gasc J, Hilairet N, Yu T et al (2017) Faulting of natural serpentinite: implications for intermediate-depth seismicity. Earth Planet Sci Lett 474:138–147

Goncharov AF, Prakapenka VB, Struzhkin VV et al (2010) X-ray diffraction in the pulsed laser heated diamond anvil cell. Rev Sci Instrum 81:5. https://doi.org/10.1063/1.3499358

Head E, Lanzirotti A, Newville M, Sutton S (2018) Vanadium, Sulfur, and Iron valences in melt inclusions as a window into magmatic processes: a case study at Nyamuragira Volcano, Africa. Geochim Cosmochim Acta 226:149–173. https://doi.org/10.1016/j.gca.2018.01.033

Heaney PJ, Oxman MJ, Chen SA (2020) A structural study of size-dependent lattice variation: in situ X-ray diffraction of the growth of goethite nanoparticles from 2-line ferrihydrite. Am Min: J Earth Planet Mater 105:652–663

Herring AL, Andersson L, Wildenschild D (2016) Enhancing residual trapping of supercritical CO2 via cyclic injections. Geophys Res Lett 43:9677–9685

Holtgrewe N, Greenberg E, Prescher C et al (2019a) Advanced integrated optical spectroscopy system for diamond anvil cell studies at GSECARS. High Press Res 39:457–470

Holtgrewe N, Greenberg E, Prescher C et al (2019b) Advanced integrated optical spectroscopy system for diamond anvil cell studies at GSECARS. High Press Res 39:457–470. https://doi.org/10.1080/08957959.2019b.1647536

Hong X, Newville M, Duffy TS et al (2013) X-ray absorption spectroscopy of GeO2glass to 64 GPa. J Phys: Condens Matter 26:035104. https://doi.org/10.1088/0953-8984/26/3/035104

Hong X, Newville M (2020) Polyamorphism of GeO2 Glass at High Pressure. Physica Status Solidi (b) 257:2000052. https://doi.org/10.1002/pssb.202000052

Incel S, Hilairet N, Labrousse L et al (2017) Laboratory earthquakes triggered during eclogitization of lawsonite-bearing blueschist. Earth Planet Sci Lett 459:320–331

Incel S, Labrousse L, Hilairet N et al (2019) Reaction-induced embrittlement of the lower continental crust. Geology 47:235–238

Jing Z, Wang Y, Kono Y et al (2014) Sound velocity of Fe–S liquids at high pressure: implications for the Moon's molten outer core. Earth Planet Sci Lett 396:78–87

Jing Z, Yu T, Xu M et al (2020) High-pressure sound velocity measurements of liquids using in situ ultrasonic techniques in a multi-anvil apparatus. Minerals 10:126. https://doi.org/10.3390/min10020126

Kantor I, Prakapenka V, Kantor A et al (2012) BX90: a new diamond anvil cell design for X-ray diffraction and optical measurements. Rev Sci Instrum 83:6. https://doi.org/10.1063/1.4768541

Kim T, Ko B, Greenberg E et al (2020) Low melting temperature of anhydrous mantle materials at the core-mantle boundary. Geophys Res Lett 47:10. https://doi.org/10.1029/2020gl089345

Kong KP, Fischer TB, Heaney PJ et al (2019) Mineralogical and geochemical constraints on chromium oxidation induced by birnessite. Appl Geochem 108:104365

Kravchenko A, Negassa W, Guber A, Rivers M (2015) Protection of soil carbon within macro-aggregates depends on intra-aggregate pore characteristics, Sci. Rep., 5, 16261. Nature Scientific Reports 5:

Lai XJ, Zhu F, Zhang JS et al (2020) An externally-heated diamond Anvil Cell for synthesis and single-crystal elasticity determination of Ice-VII at high pressure-temperature conditions. J vis Exp 160:14. https://doi.org/10.3791/61389

Lanzirotti A, Dyar MD, Sutton S et al (2018) Accurate predictions of microscale oxygen barometry in basaltic glasses using V K-edge X-ray absorption spectroscopy: a multivariate approach. Am Miner 103:1282–1297. https://doi.org/10.2138/am-2018-6319

Lesher CE, Wang Y, Gaudio S et al (2009) Volumetric properties of magnesium silicate glasses and supercooled liquid at high pressure by X-ray microtomography. Phys Earth Planet Inter 174:292–301

Lv M, Dorfman SM, Badro J et al (2021) Reversal of carbonate-silicate cation exchange in cold slabs in Earth's lower mantle. Nat Commun 12:7. https://doi.org/10.1038/s41467-021-21761-9

McBriarty ME, von Rudorff GF, Stubbs JE et al (2017) Dynamic stabilization of metal oxide–water interfaces. J Am Chem Soc 139:2581–2584

McBriarty ME, Stubbs JE, Eng PJ, Rosso KM (2018a) Potential-specific structure at the hematite-electrolyte interface. Adv Func Mater 28:1705618

McBriarty ME, Stubbs JE, Eng PJ, Rosso KM (2018b) Reductive dissolution mechanisms at the hematite-electrolyte interface probed by in situ X-ray scattering. J Phys Chem C 123:8077–8085

Neumann J, Qiu C, Eng P et al (2021) Effect of background electrolyte composition on the interfacial formation of Th (IV) nanoparticles on the muscovite (001) basal plane. J Phys Chem C 125:16524–16535

Nishiyama N, Wang Y (2009) Development of Experimental Techniques Using LVP (Large Volume Press) at GSECARS Beamlines, Advanced Photon Source (in Japanese with English abstract). Rev High Pressure Sci Tech 18:

Phillips-Lander CM, Harrold Z, Hausrath EM et al (2020) Snow Algae Preferentially Grow on Fe-containing Minerals and Contribute to the Formation of Fe Phases. Geomicrobial J 37:572–581. https://doi.org/10.1080/01490451.2020.1739176

Pichavant M, Brugier Y, Muro AD (2016) Petrological and experimental constraints on the evolution of Piton de la Fournaise magmas. In: Active Volcanoes of the Southwest Indian Ocean. Springer, pp 171–184

Prakapenka VB, Shen GY, Rivers ML et al (2005) Grain-size control in situ at high pressures and high temperatures in a diamond-anvil cell. J Synchrot Radiat 12:560–565. https://doi.org/10.1107/s0909049505021928

Prakapenka VB, Kubo A, Kuznetsov A et al (2008) Advanced flat top laser heating system for high pressure research at GSECARS: application to the melting behavior of germanium. High Press Res 28:225–235

Prakapenka VB, Holtgrewe N, Lobanov SS, Goncharov AF (2021) Structure and properties of two superionic ice phases. Nat Phys 17:1233. https://doi.org/10.1038/s41567-021-01351-8

Prescher C, Prakapenka VB (2015) DIOPTAS: a program for reduction of two-dimensional X-ray diffraction data and data exploration. High Press Res 35:223–230

Qiu C, Majs F, Douglas TA et al (2018a) In situ structural study of Sb (V) adsorption on hematite $(1\bar{1}02)$ using X-ray surface scattering. Environ Sci Technol 52:11161–11168

Qiu C, Majs F, Eng PJ et al (2018b) In situ structural study of the surface complexation of lead (II) on the chemically mechanically polished hematite (11 02) surface. J Colloid Interface Sci 524:65–75

Redmer R, Mattsson TR, Nettelmann N, French M (2011) The phase diagram of water and the magnetic fields of Uranus and Neptune. Icarus 211:798–803

Rivers M, Prakapenka VB, Kubo A et al (2008) The COMPRES/GSECARS gas-loading system for diamond anvil cells at the Advanced Photon Source. High Press Res 28:273–292

Rivers ML, Wang Y (2006) Recent developments in microtomography at GeoSoilEnviroCARS. In: Developments in X-ray tomography V. SPIE, pp 156–170

Rivers ML, Sutton SR, Eng PJ (1999) Geoscience applications of X-ray computed microtomography. In: Developments in X-ray Tomography II. International Society for Optics and Photonics, pp 78–86

Rivers ML, Citron DT, Wang Y (2010) Recent developments in computed tomography at GSECARS. In: Developments in X-Ray Tomography VII. SPIE, pp 83–97

Rivers ML (2012) tomoRecon: High-speed tomography reconstruction on workstations using multi-threading. In: Developments in X-Ray Tomography VIII. SPIE, pp 169–181

Rivers ML (2016) High-speed tomography using pink beam at GeoSoilEnviroCARS. In: Developments in X-ray Tomography X. International Society for Optics and Photonics, p 99670X

Sanematsu P, Shen Y, Thompson K et al (2015) Image-based stokes flow modeling in bulk proppant packs and propped fractures under high loading stresses. J Petrol Sci Eng 135:391–402

Schmidt M, Eng PJ, Stubbs JE et al (2011) A new x-ray interface and surface scattering environmental cell design for in situ studies of radioactive and atmosphere-sensitive samples. Rev Sci Instrum 82:075105

Schubnel A, Brunet F, Hilairet N et al (2013) Deep-focus earthquake analogs recorded at high pressure and temperature in the laboratory. Science 341:1377–1380

Shen GY, Prakapenka VB, Rivers ML, Sutton SR (2004) Structure of liquid iron at pressures up to 58 GPa. Phys Rev Lett 92:4. https://doi.org/10.1103/PhysRevLett.92.185701

Shi F, Wang Y, Yu T et al (2018) Lower-crustal earthquakes in southern Tibet are linked to eclogitization of dry metastable granulite. Nat Commun 9:1–13

Shi WG, Sun NY, Li XY et al (2021) Single-crystal elasticity of high-pressure ice up to 98 GPa by Brillouin Scattering. Geophys Res Lett 48:11. https://doi.org/10.1029/2021gl092514

Shi F, Wang Y, Wen J et al (2022) Metamorphism-facilitated faulting in deforming orthopyroxene: implications for global intermediate-depth seismicity. Proc Natl Acad Sci 119:e2112386119

Sinogeikin S, Bass J, Prakapenka V et al (2006a) Brillouin spectrometer interfaced with synchrotron radiation for simultaneous X-ray density and acoustic velocity measurements. Rev Sci Instrum 77:103905

Socha AL, Guerinot ML (2014) Mn-euvering manganese: the role of transporter gene family members in manganese uptake and mobilization in plants. Front Plant Sci 5:106

Stack AG, Stubbs JE, Srinivasan SG et al (2018) Mineral-water interface structure of Xenotime (YPO4){100}. J Phys Chem C 122:20232–20243

Stubbs JE, Chaka AM, Ilton ES et al (2015) UO 2 oxidative corrosion by nonclassical diffusion. Phys Rev Lett 114:246103

Stubbs JE, Legg BA, Lee SS et al (2019) Epitaxial growth of gibbsite sheets on the basal surface of muscovite mica. J Phys Chem C 123:27615–27627

Stubbs JE, Wanhala AK, Eng PJ (2021) Interfacial X-Ray Scattering from Small Surfaces: Adapting Mineral-Fluid Structure Methods for Microcrystalline Materials. Clays Clay Miner 69:1–14

Sutton SR, Karner J, Papike J et al (2005) Vanadium K edge XANES of synthetic and natural basaltic glasses and application to microscale oxygen barometry. Geochim Cosmochim Acta 69:2333–2348

Sutton SR, Brearley AJ, DobricĂ E et al (2020a) Valence determinations and oxybarometry on FIB-sectioned olivine and pyroxene using correlated Ti, V, and Cr micro-XAFS spectroscopy: evaluation of ion-milling effects and application to Antarctic micrometeorite grains. Meteorit Planet Sci 55:2553–2569. https://doi.org/10.1111/maps.13603

Sutton SR, Lanzirotti A, Newville M et al (2020b) Oxybarometry and valence quantification based on microscale X-ray absorption fine structure (XAFS) spectroscopy of multivalent elements. Chem Geol 531:119305

Tinker D, Lesher CE, Baxter GM et al (2004) High-pressure viscometry of polymerized silicate melts and limitations of the Eyring equation. Am Miner 89:1701–1708

Todd KA, Watson HC, Yu T, Wang Y (2016) The effects of shear deformation on planetesimal core segregation: results from in-situ X-ray micro-tomography. Am Miner 101:1996–2004

Tschauner O, Huang S, Greenberg E et al (2018) Ice-VII inclusions in diamonds: evidence for aqueous fluid in Earth's deep mantle. Science 359:1136. https://doi.org/10.1126/science.aao3030

Wang Y, Uchida T, Westferro F et al (2005) High-pressure x-ray tomography microscope: synchrotron computed microtomography at high pressure and temperature. Rev Sci Instrum 76:073709

Wang Y, Rivers M, Sutton S et al (2009) The large-volume high-pressure facility at GSECARS: a "Swiss-army-knife" approach to synchrotron-based experimental studies. Phys Earth Planet Inter 174:270–281. https://doi.org/10.1016/j.pepi.2008.06.017

Wang Y, Lesher C, Fiquet G et al (2011) In situ high-pressure and high-temperature X-ray microtomographic imaging during large deformation: a new technique for studying mechanical behavior of multiphase composites. Geosphere 7:40–53

Wang Y, Sakamaki T, Skinner LB et al (2014) Atomistic insight into viscosity and density of silicate melts under pressure. Nat Commun 5:1–10

Wang Y, Gélabert A, Michel FM et al (2016a) Effect of biofilm coatings at metal-oxide/water interfaces I: Pb (II) and Zn (II) partitioning and speciation at Shewanella oneidensis/metal-oxide/water interfaces. Geochim Cosmochim Acta 188:368–392

Wang Y, Gélabert A, Michel FM et al (2016b) Effect of biofilm coatings at metal-oxide/water interfaces II: competitive sorption between Pb (II) and Zn (II) at Shewanella oneidensis/metal-oxide/water interfaces. Geochim Cosmochim Acta 188:393–406

Wang Y, Michel FM, Choi Y et al (2016c) Pb, Cu, and Zn distributions at humic acid-coated metal-oxide surfaces. Geochim Cosmochim Acta 188:407–423

Wang Y, Zhu L, Shi F et al (2017) A laboratory nanoseismological study on deep-focus earthquake micromechanics. Sci Adv 3:e1601896

Wenz MD, Jacobsen SD, Zhang D et al (2019) Fast identification of mineral inclusions in diamond at GSECARS using synchrotron X-ray microtomography, radiography and diffraction. J Synchrotron Radiat 26:1763–1768

Xu M, Jing Z, Chantel J et al (2018) Ultrasonic velocity of diopside liquid at high pressure and temperature: constraints on velocity reduction in the upper mantle due to partial melts. J Geophys Res: Solid Earth 123:8676–8690

Xu T, Stubbs JE, Eng PJ, Catalano JG (2019) Comparative response of interfacial water structure to pH variations and arsenate adsorption on corundum (0 1 2) and (0 0 1) surfaces. Geochim Cosmochim Acta 246:406–418

Xu M, Jing Z, Bajgain SK et al (2020a) High-pressure elastic properties of dolomite melt supporting carbonate-induced melting in deep upper mantle. Proc Natl Acad Sci USA 117:18285. https://doi.org/10.1073/pnas.2004347117

Xu M, Jing Z, Van Orman JA et al (2020b) Density of NaAlSi2O6 Melt at high pressure and temperature measured by In-Situ X-ray Microtomography. Minerals 10:161. https://doi.org/10.3390/min10020161

Xu M, Jing Z, Yu T et al (2022) Sound velocity and compressibility of melts along the hedenbergite (CaFeSi2O6)-diopside (CaMgSi2O6) join at high pressure: implications for stability and seismic signature of Fe-rich melts in the mantle. Earth Planet Sci Lett 577:117250

Yu T, Prescher C, Ryu YJ et al (2019a) A Paris-Edinburgh cell for high-pressure and high-temperature structure studies on silicate liquids using monochromatic synchrotron radiation. Minerals 9:715. https://doi.org/10.3390/min9110715

Yu T, Wang Y, Rivers ML, Sutton SR (2019b) An upgraded and integrated large-volume high-pressure facility at the GeoSoilEnviroCARS bending magnet beamline of the Advanced Photon Source. CR Geosci 351:269–279. https://doi.org/10.1016/j.crte.2018.09.006

Yuan HS, Zhang L, Ohtani E et al (2019) Stability of Fe-bearing hydrous phases and element partitioning in the system MgO-Al2O3-Fe2O3-SiO2-H2O in Earth's lowermost mantle. Earth Planet Sci Lett 524:10. https://doi.org/10.1016/j.epsl.2019.115714

Zinin PV, Prakapenka VB, Burgess K et al (2016) Combined laser ultrasonics, laser heating, and Raman scattering in diamond anvil cell system. Rev Sci Instrum 87:123908

Publisher's Note Springer Nature remains neutral with regard to jurisdictional claims in published maps and institutional affiliations.